

A Detailed Geochemical Study of a Shallow Arc-related Laccolith; the Torres del Paine Mafic Complex (Patagonia)

J. LEUTHOLD^{1*}, O. MÜNTENER¹, L. P. BAUMGARTNER¹,
B. PUTLITZ¹ AND M. CHIARADIA²

¹INSTITUTE OF MINERALOGY AND GEOCHEMISTRY, UNIVERSITY OF LAUSANNE, 1015 LAUSANNE, SWITZERLAND

²SECTION OF EARTH AND ENVIRONMENTAL SCIENCES, UNIVERSITY OF GENEVA, 1205 GENEVA, SWITZERLAND

RECEIVED AUGUST 29, 2011; ACCEPTED SEPTEMBER 7, 2012
ADVANCE ACCESS PUBLICATION NOVEMBER 3, 2012

The shallow crustal Torres del Paine Intrusive Complex in southern Patagonia offers an opportunity to understand the chemical evolution and timing of crystallization processes in shallow plutonic rocks. It is characterized by hornblende-gabbros, gabbronorites, monzodiorites and granitic plutonic rocks. The exceptional exposure of the intrusion permits the identification of two structurally and petrographically different zones. Layered gabbronorite, olivine-bearing pyroxene-hornblende gabbronorite and monzodiorite forming vertical sheets and stocks in the west are referred to here as the feeder zone. These mafic rocks are in vertical contact with younger granitic rocks on their eastern border. The eastern part is a laccolith complex. It is characterized by three major units (I, II, III) of granitic rocks of over 1000 m vertical thickness; these are underlain in places by a sequence of hornblende-gabbro sills intermingled with evolved monzodiorite granite. Chilled, crenulated margins as well as flame structures between gabbroic rocks and monzodiorites suggest that the mafic sill complex remained partially molten during most of its construction. Bulk-rock major and trace element data indicate that the Paine mafic rocks follow a high-K calc-alkaline to shoshonitic differentiation trend. The parental magmas were basaltic trachyandesite liquids, with variable H₂O and alkali contents. The majority of the feeder zone gabbronorites have high Al₂O₃ contents and positive Eu and Sr anomalies, consistent with accumulation of plagioclase and efficient extraction of intercumulus melt. The mafic sill complex largely lacks these cumulate signatures. Comparisons of the intercumulus groundmass in the hornblende-gabbros with intra-sill dioritic stocks and pods reveal similar rare earth element patterns and trace element ratios indicating incomplete extraction of evolved interstitial liquids. The Sr, Nd and Pb isotopic compositions of the mafic and

granitic rocks exhibit ranges of ⁸⁷Sr/⁸⁶Sr of 0.704–0.708, εNd +3.8 to –1.2, ²⁰⁶Pb/²⁰⁴Pb 18.61–18.77, ²⁰⁷Pb/²⁰⁴Pb 15.67–15.67 and ²⁰⁸Pb/²⁰⁴Pb 38.56–38.77. Crystal fractionation and assimilation-fractional crystallization modelling, combined with high-precision U–Pb dating of zircons, indicates that the western feeder zone gabbronorites are linked to the uppermost Paine granite (granite I), whereas the mafic sill complex is younger and not directly related to the voluminous granite units II and III. These results are interpreted to indicate that crystal-liquid separation is facilitated in subvertical, dynamic feeder systems whereas subhorizontal sill complexes are inefficient in separating large volumes of mafic cumulates and complementary felsic rocks.

KEY WORDS: crystal fractionation; granite-mafic laccolith; high-K calc-alkaline magmatism; Chile; Patagonia; Torres del Paine

INTRODUCTION

Fractional crystallization and assimilation models (DePaolo, 1981; Hildreth & Moorbath, 1988; Davidson *et al.*, 1990; Mason *et al.*, 1996; Knesel *et al.*, 1999; Glazner & Bartley, 2006; Glazner, 2007), experiments on liquid line of descent, cumulate formation (Müntener & Ulmer, 2006), and partial melting experiments (Sisson *et al.*, 2005) show that felsic liquids typically represent less than ~50% of the mass of the parent liquid originally in equilibrium with mantle peridotite. Hence large volumes of mafic rocks should have accumulated at depth in order to

*Corresponding author. Present address: School of Earth Sciences, University of Bristol, Wills Memorial Building, Bristol BS8 1RJ, UK. Telephone: +44 (0)117 331 5181. Fax: +44 (0)117 925 3385. E-mail: julien.leuthold@bristol.ac.uk

obtain a continental upper crust with a mean composition of granodiorite from basalts injected into the lower continental crust. Many crustal plutonic complexes are built by the amalgamation of successive magma batches or pulses (e.g. Glazner *et al.*, 2004; Miller, J. S., *et al.*, 2007; Michel *et al.*, 2008; Horsman *et al.*, 2010; Miller, C. F., *et al.*, 2011), such that it may take several tens of thousands to millions of years to develop from an single pluton to a batholith (de Saint-Blanquat *et al.*, 2011). Small volumes of differentiated melt can be extracted from a crystal mush, leaving a residual mafic cumulate, and emplaced as a succession of pulses, progressively building up the growing magma body (e.g. Sisson *et al.*, 1996).

Assimilation–fractional crystallization (AFC) models provide a means to identify potential genetic links between single magmatic units. The scarcity of intermediate magmas in bimodal plutons, the ‘Daly Gap’ (Daly, 1925), is an important constraint on the chemical evolution from mafic to felsic magmas. Although such bimodality may be explained by partial melting of mafic rocks at depth (e.g. Petford *et al.*, 1996; Sisson *et al.*, 2005), the fractionation of SiO₂-poor minerals such as olivine, hornblende and Fe–Ti oxides is an efficient means to fractionate primitive liquids towards more silicic compositions. The necessary large volumes of ultramafic to mafic cumulates (Müntener *et al.* 2001; Sisson *et al.*, 2005), required to build derivative silicic magmas, are preserved in the lower crust and/or shallower plutons (Ulmer *et al.*, 1983; Kemp, 2004; Jagoutz, 2010). In particular, hornblende and hornblende-gabbro cumulates are common throughout the crust (Debari *et al.*, 1987; Sisson *et al.*, 1996; Davidson *et al.*, 2007; Larocque & Canil, 2010; Dessimoz *et al.*, 2012). Parts of these mafic rocks can be remobilized as xenocrysts and xenoliths (Dungan & Davidson, 2004).

The Torres del Paine Intrusive Complex (TPIC) is a bimodal felsic–mafic shallow crustal laccolith connected to a subvertical feeding system (Michael, 1984, 1991; Baumgartner *et al.*, 2007; Michel *et al.*, 2007, 2008; Leuthold *et al.*, 2012). The spectacular outcrops across the laccolith and its feeder zone provide an opportunity to study the relationships between the subvertical feeding system and the subhorizontal sill complex. Combined with high-precision dating (Michel *et al.*, 2008; Leuthold *et al.*, 2012), links are proposed between the primitive mafic and evolved magmas. Here, we present in detail the geochemical variations within single TPIC mafic units and discuss their genetic link with the associated granitic rocks described by Michael (1984), Baumgartner *et al.* (2007), and Michel *et al.* (2008). We first present bulk-rock major and trace element and Sr, Nd and Pb isotope data, then we constrain the primitive liquid compositions using bulk-rock analyses of mafic dikes. Using recent, high-precision, U–Pb dating of zircons (Michel *et al.*, 2008; Leuthold *et al.*, 2012) combined with the geochemical data, we show that the mafic

complex consists of different differentiation series, which link the laccolith gabbros and monzodiorites, as well as gabbros from the feeder zone, to the oldest granitic unit. We go on to show that AFC models fail to reproduce the isotopic composition of the Paine granites using the mafic dikes as the starting magma composition combined with variable amounts of assimilated wall-rock consisting of either the Jurassic batholith (Hervé *et al.*, 2007), Patagonian S-type crust (Kilian & Behrmann, 2003), or Paleozoic metamorphic basement (Pankhurst *et al.*, 2003).

Combining field observations, microtextural analyses, geochemical data and U–Pb zircon ages, we show that felsic liquids are incompletely separated from mafic cumulates during magma ascent.

GEOLOGICAL SETTING AND PREVIOUS WORK

The TPIC is emplaced into early to mid-Cretaceous continental and shallow marine pelitic to psammitic rocks (Cerro Toro and Punta Barossa formations, Wilson, 1983) (Fig. 1). It belongs to a chain of isolated Miocene plutons (Co. Pinto, Co. Balmaceda, Co. Donoso, Co. Fitz Roy and Co. San Lorenzo) and subvolcanic rocks (Michael, 1991). These plutons are located in a transitional position between the generally older calc-alkaline Patagonian Batholith in the west and the younger alkaline plateau basalts in the east (Fig. 1). A recent description of the petrology and geology of the TPIC can be found in the field guide distributed on the occasion of the GEOSUR excursion to the Torres del Paine (Baumgartner *et al.*, 2007). Estimates of the emplacement depth of the TPIC (Putlitz *et al.*, 2001), based on fluid inclusions and the observed prehnite–plagioclase assemblages in the contact-metamorphosed country-rocks, yielded 75 ± 30 MPa as the maximum pressure during contact metamorphism. The TPIC laccolith is spectacularly exposed in three dimensions as a result of subsequent Quaternary glacial erosion, with over 1000 m high vertical granitic cliffs, which overlie ~250 m of gabbroic and dioritic rocks in the central part of the TPIC. The total volume is estimated to be ~88 km³ (Leuthold *et al.*, 2012).

The TPIC is a bimodal igneous body, built up by multiple pulses of mafic and felsic magmas. In its western part, it has steep, subvertical structures, generally discordant to the folded country-rocks; this is referred to as the feeder zone (FZ), following Baumgartner *et al.* (2007) and Michel *et al.* (2008). The eastern part is a laccolith (LA), with subhorizontal contacts between distinct units (Fig. 2). The TPIC laccolith consists of a basal mafic sill complex and the overlying Paine granite (Michael, 1984, 1991; Baumgartner *et al.*, 2006, 2007; Michel *et al.*, 2007, 2008). The mafic rocks of the laccolith and the feeder zone form

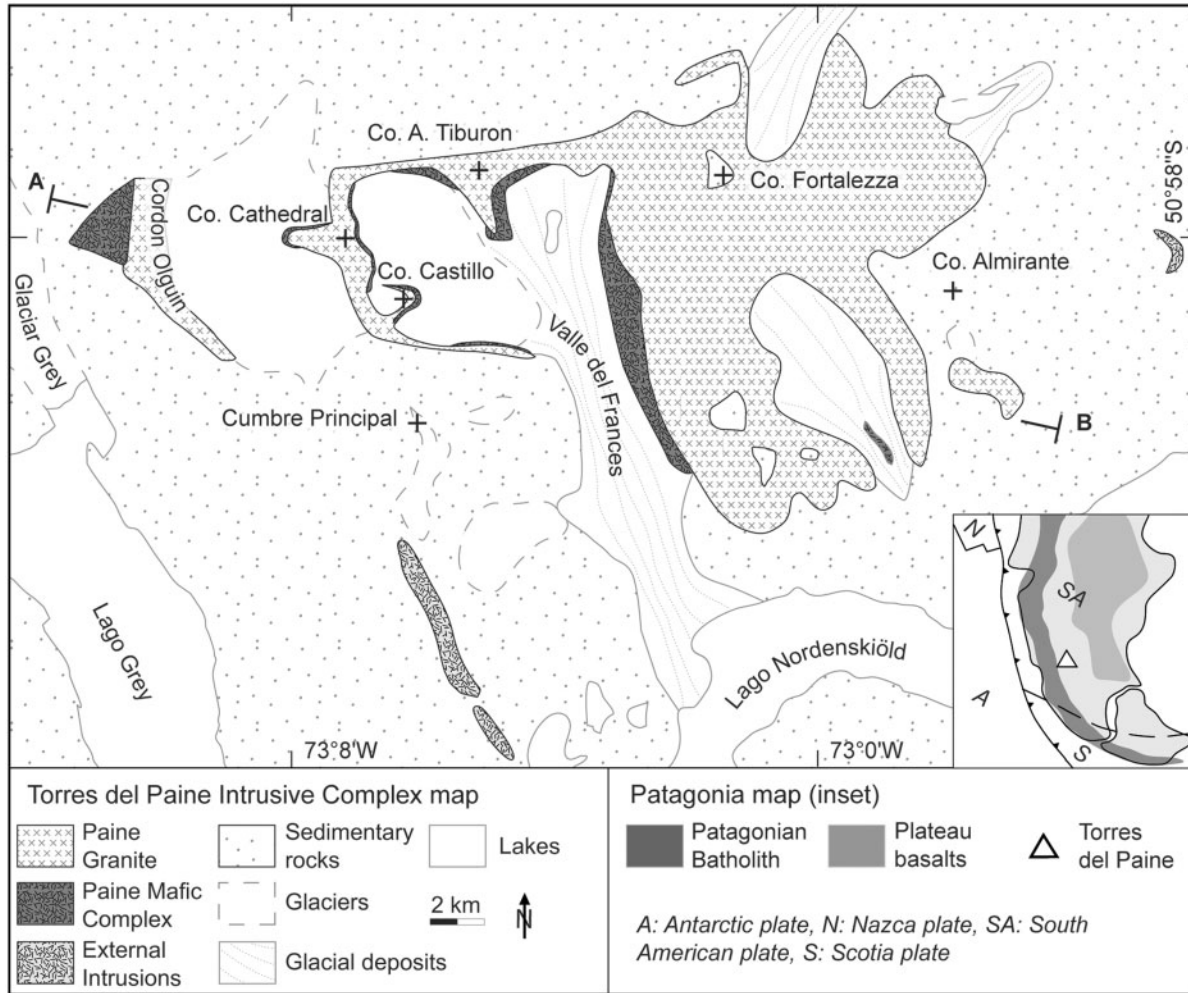


Fig. 1. Geological map of the Torres del Paine intrusive complex (TPIC). Igneous contacts between intrusive units, as well as with the host-rock, are steep in the west, whereas they are generally subhorizontal in the central and eastern parts. Modified after Michel *et al.* (2008). The inset map places the TPIC (triangle) in the regional context.

the Paine Mafic Complex (PMC). This nomenclature and subdivisions will be retained in the following discussion.

Based on field observations of the laccolith it has been proposed that a high-K basaltic trachyandesite liquid intruded into partly crystalline granitic rocks (Michael, 1991), with sharp contacts. Assuming consanguinity and contemporaneity of the Paine felsic and mafic magmas, Michael (1984) explained their chemical evolution in terms of closed-system *in situ* crystallization into two separate convecting and differentiating systems. Michael (1991) suggested that the granitic magmas were derived in some way from mafic magmas similar to those that formed the associated mafic complex. He proposed that fractional crystallization of olivine, Ca-rich plagioclase, pyroxene and hornblende from a basaltic liquid formed the observed intermediate rocks preserved within the mafic complex. Recent high-precision U–Pb thermal ionization mass spectrometry (TIMS) dating (Michel *et al.*, 2008; Leuthold

et al., 2012) has, however, allowed us to re-evaluate the links between the mafic and felsic magmas.

Geochronological studies indicate that the granitic magmas were emplaced over a short time interval of ~90 kyr during the Miocene (Michel *et al.*, 2008), and the whole TPIC was built up over 162 ± 11 kyr (Leuthold *et al.*, 2012). Two dated samples from the feeder zone mafic complex have ages similar to the oldest Unit I granite. In contrast, dated samples of the mafic sill complex are all younger than the overlying granite. Slightly older zircon grains than the youngest cluster age are common in dated TPIC granitic and mafic samples, with age differences as high as 20–30 kyr (Leuthold *et al.*, 2012). These have been interpreted to be antecrysts. Calc-alkaline gabbros from the external intrusions (Fig. 1), which are not co-genetic with the TPIC (Quensel, 1911; Michael, 1991), have been dated at 16.8 ± 0.3 Ma (Fosdick *et al.*, 2011) and 29.4 ± 0.8 Ma (Altenberger *et al.*, 2003).

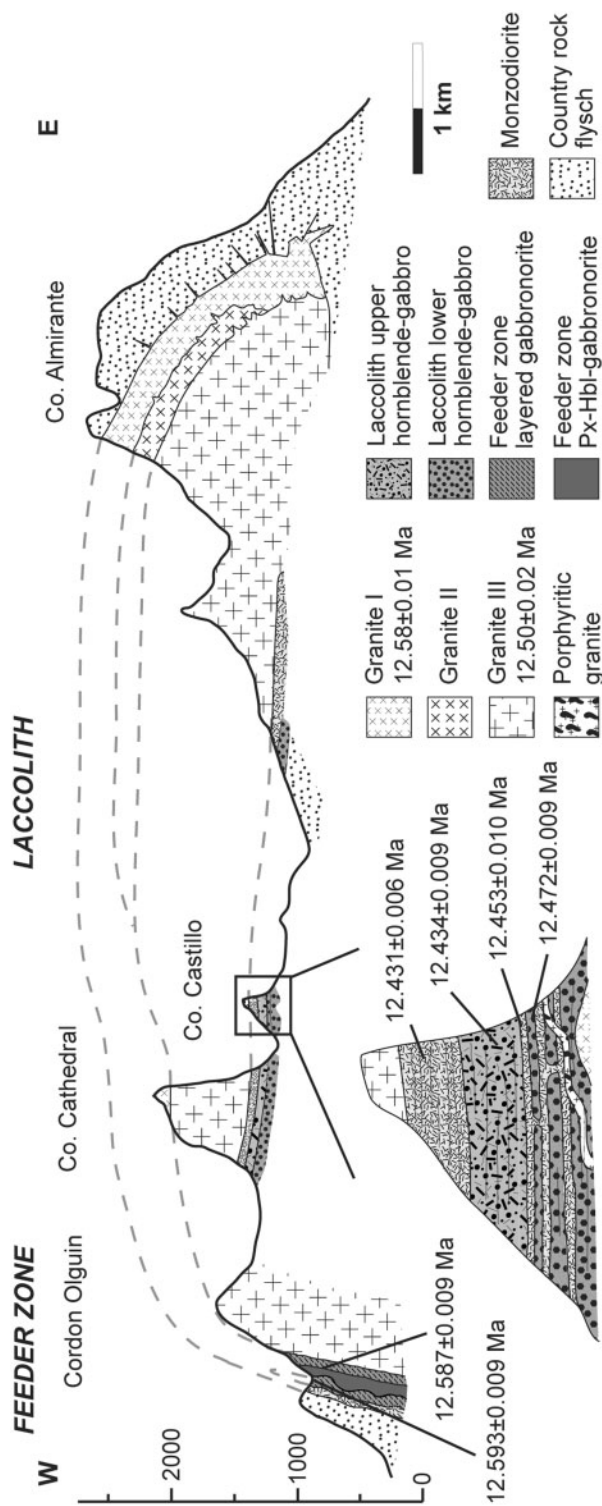


Fig. 2. A west-east cross-section through the TPIC, showing the PMC and the granitic complex (profile A–B in Fig. 1). Modified after Leuthold *et al.* (2012). The feeder zone (FZ) in the west has subvertical internal structures, both in the granitic and the mafic rocks, whereas the eastern part is a laccolith (LA) composed of horizontal sheets and sills. The PMC is overlain by ~1000–1500 m of granitic rocks in the central part.

FIELD RELATIONS

Feeder zone (FZ)

Field work carried out over the past 8 years by a group from Lausanne University has revealed that the western part of the TPIC is characterized by steep contacts over an area of ~4 km². Five igneous rock units can be distinguished.

(1) Layered gabbronorite

Coarse-grained gabbronorites show alternating plagioclase-rich and orthopyroxene ± clinopyroxene-rich, centimetre thick layers (Fig. 3a) that can be followed laterally over a few tens of metres. The layering is subvertical, although locally there is evidence of ductile deformation. Spectacular truncations between adjacent layers produce structures that are similar to the forest structures seen in sedimentary rocks. The pyroxene and plagioclase modal content is highly variable. A pegmatite from this unit has been dated by isotope dilution (ID)-TIMS at 12.587 ± 0.009 Ma (Leuthold *et al.*, 2012). Country-rock metasedimentary marl and quartzite xenoliths are generally rare, but may form up to ~5 vol. % locally. All the xenoliths are oriented parallel to the layered gabbronorite structures; they are often stretched (Fig. 3b), rarely folded and may display partial melting features. Their exact origin is so far unknown; nevertheless, pelites, sandstones and some calcareous layers occur in the Punta Barrosa and Cerro Toro formations (Baumgartner *et al.*, 2007).

(2) Pyroxene–hornblende gabbronorite

Together with the layered gabbronorite, pyroxene–hornblende gabbronorite forms a succession of ~20 m thick east–west-trending vertical stocks [as defined by Jackson & Pollard (1988)]. Homogeneous FZ pyroxene–hornblende gabbronorite plugs display sharp and locally sinuous contacts with the layered gabbronorites (Fig. 3c) and their included metasedimentary xenoliths. This unit has been dated at 12.593 ± 0.009 Ma (Leuthold *et al.*, 2012).

(3) Monzodiorite

Hornblende-bearing biotite monzodiorite is exposed in the northern, eastern and southern border of the feeder zone. Contacts with older FZ pyroxene–hornblende gabbronorite and layered gabbronorite are sharp to ductile (Fig. 3d). Layered gabbronorite xenoliths are locally observed. Monzodiorite truncates deformed, layered gabbronorite in the central part of the FZ (Fig. 3d).

(4) Unit III granite

A homogeneous, medium-grained biotite–hornblende granite is found in the eastern part of the feeder zone, and constitutes the Cordon Olguin crest (Fig. 1). It has been dated by Michel *et al.* (2008) at 12.50 ± 0.02 Ma [recalculated by Leuthold *et al.* (2012), containing an antecryst dated at 12.54 ± 0.03 Ma]. This is part of the youngest of

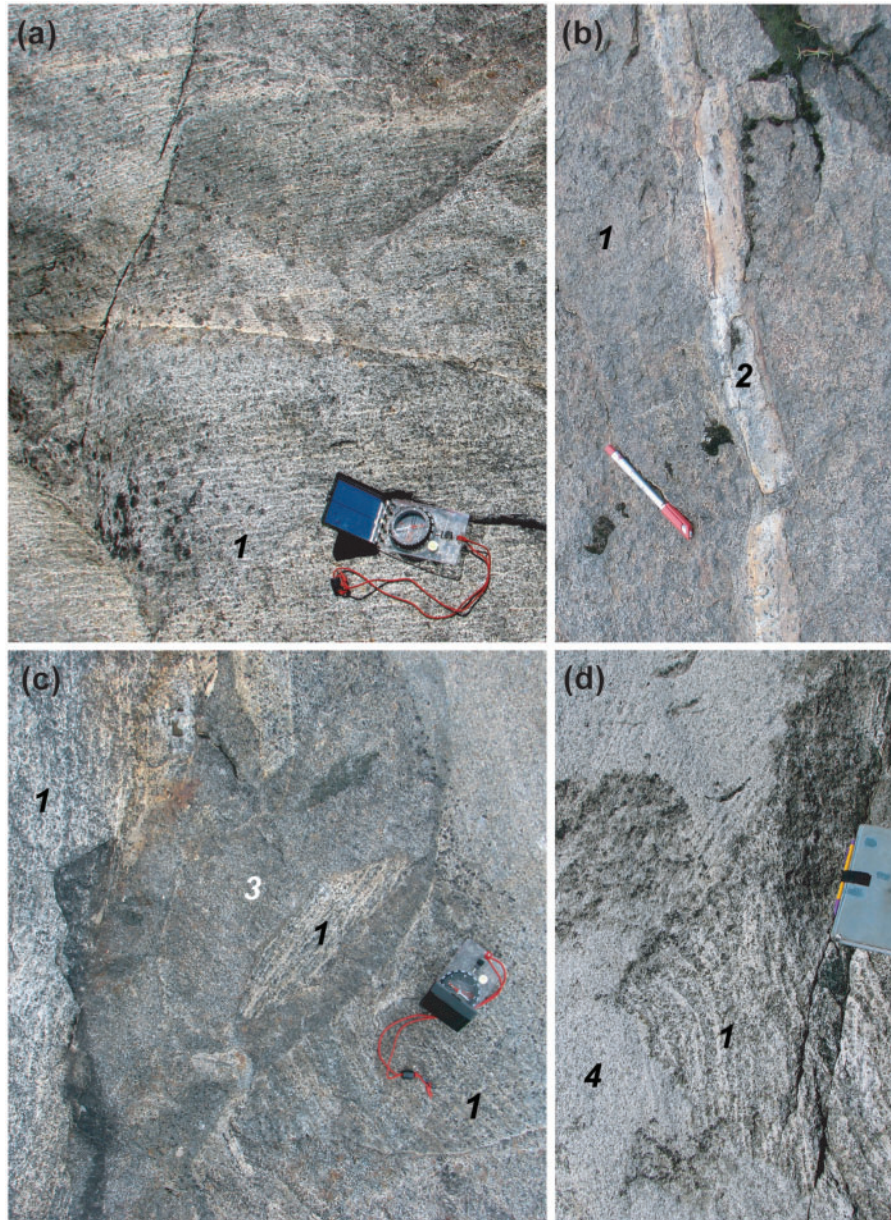


Fig. 3. Field photographs of the TPIC feeder zone. (a) Layered gabbronorite, with centimetre-thick, leucocratic, plagioclase-rich zones alternating with mesocratic, pyroxene-rich zones. The layering is continuous for metres or tens of metres. (b) Disintegrated layers of quartzite are caught up in the layered gabbronorite. (c) Sharp intrusive contacts between pyroxene-hornblende-gabbronorite intruded into layered gabbronorite. (Note the angular xenolith of layered gabbronorite, documenting the brittle nature of the contact.) (d) Intrusion of monzodiorite into layered gabbronorite with irregular contact. 1, Layered gabbronorite; 2, quartzite layer; 3, pyroxene-hornblende gabbronorite; 4, monzodiorite.

the three major granite sheets (unit III, Michel *et al.*, 2008) that build up the TPIC granitic bodies.

(5) *Porphyritic granite*

The youngest plutonic rocks in the feeder zone are metre- to decametre-scale enclave-rich (20–50%) porphyritic granites that mainly follow the sediment-gabbronorite contact, and form discrete dikes that cross-cut all other plutonic rocks. They show sharp, brittle contacts with the surrounding

gabbronorite, locally accompanied by the formation of a dense, centimetre-thick fracture networks. Large (1–10 m) quenched enclaves are mainly of dioritic composition. These show cauliflower-like, lobate contacts and sometimes exhibit brittle fractures filled with porphyritic granite melt.

Laccolith (LA)

The laccolithic mafic complex formed in at least three major episodes. Rocks of these three episodes are cut by

an enclave-rich, porphyritic granite that is similar to the porphyritic granite of the feeder zone (see above). The mafic sill complex is on average 300 m thick (Fig. 4a and b). It is formed of (monzo-)gabbros and monzodiorites, and is overlain by over 1000 m of granite, which was amalgamated in at least three major intrusive events (e.g. Michel *et al.*, 2008). In the following, the term gabbro is used *senso lato* to include monzogabbros and gabbros.

(1) Lower hornblende-gabbro

The lower mafic unit is an olivine-bearing, biotite–hornblende-gabbro to hornblende-phyric monzonite. It is formed of 30–60 m thick sills (Fig. 4b). This unit has been dated by Leuthold *et al.* (2012) at 12.472 ± 0.009 Ma. The mafic sills frequently display mineralogical and textural gradations. An ~30 m thick sill at the base of Co. Aleta de Tiburon (see Fig. 1 for location) grades from a melanocratic hornblende-gabbro in the centre to equigranular monzodiorite, and finally granodiorite with acicular biotite and phenocrysts of K-feldspar towards the top and the bottom margin. Similar observations were made at the base of Co. Castillo.

(2) Upper hornblende-gabbro

The lower mafic unit is overlain by the upper (olivine-bearing) hornblende-gabbro, characterized by euhedral plagioclase inclusions in poikilitic hornblende. The crystallization age is 12.433 ± 0.009 Ma, according to Leuthold *et al.* (2012). This also comprises a number of sills ~20 m thick. Contacts are difficult to locate exactly because of progressive mineralogical, modal and grain-size variations over a few metres. In the upper hornblende-gabbro the modal amount of large (centimetre-scale) mafic minerals decreases from the base to the top of the sill. No direct field relations are observed between the two hornblende-gabbro units, as the contacts are always separated by monzodiorite sills. Subhorizontal, schlieren-like textures, defined by concentrations of hornblende, are found in both hornblende-gabbros. At Co. Castillo a 5 cm thick hornblende-rich (hornblendite) subhorizontal layer displays ductile deformation and syn-magmatic shear folding. At Co. Aleta de Tiburon (Fig. 1), similar hornblendite bodies have been deformed and left as 'ductile boudins' in a fine-grained monzodiorite host.

(3) Monzodiorites

Two types of monzodiorite can be distinguished in the laccolith, based on field observations.

(a) Thin, 1 to >5 m thick monzodiorite sills with variable hornblende/biotite ratios are found at the very top of the mafic complex, where they form a coherent, mappable unit. Within the lower 30 m of this unit, single monzodiorite sills become gradually more leucocratic upwards, with acicular biotite and/or hornblende and rare phenocryst K-feldspar and/or quartz. The uppermost monzodiorite

has been dated at 12.431 ± 0.006 Ma by Leuthold *et al.* (2012). Pegmatitic varieties are frequently observed along the roof zone. A few pegmatoid pods have a granodioritic mineralogical composition. No chilled margins are observed along their sharp, but sinuous contacts. The upper 20 m in contact with the overlying Paine granite is characterized by the presence of elongated monzodioritic enclaves (10 m long, ~1 m thick), surrounded by quartz-bearing granite with ~1 cm K-feldspar phenocrysts (Fig. 4b and c).

(b) Monzodiorites also form interconnected sills in the hornblende-gabbro units. These sills have irregular and complex boundaries with the surrounding mafic sheets. Many contacts are texturally and compositionally heterogeneous, with the monzodiorites containing gabbroic enclaves and/or macrocrystals. Centimetre-scale granodioritic diapirs occasionally ascend from the dioritic sills into the (at the time) partially crystallized, overlying gabbroic unit. Mirolitic cavities are frequent in such diapirs. The monzodiorite sill between the lower and upper hornblende-gabbro units in the Co. Castillo outcrop has been dated at 12.453 ± 0.010 Ma (Leuthold *et al.*, 2012).

(4–6) Units I, II and III granite

At least three units have been distinguished in the Paine granite and described by Baumgartner *et al.* (2007), Michel *et al.* (2008) and Michel *et al.* (2006). The uppermost one consists of a silica-rich, hornblende-bearing, biotite-granite (Unit I granite). This unit reaches a thickness of over 800 m in the east, whereas it is much thinner (~200 m) in the central part of the laccolith. It has been dated at 12.58 ± 0.01 Ma (Michel *et al.*, 2008). The ages reported here have been recalculated by Leuthold *et al.* (2012) to obtain a coherently treated age dataset for the TPIC rocks. Two antecrysts have slightly older ages of 12.63 ± 0.03 and 12.61 ± 0.03 Ma. The Unit I granite is intruded by an ~200–400 m thick medium-grained, biotite–hornblende granite, which contains many metre-scale mafic enclaves (Unit II granite) and also some mafic clots. This unit is itself intruded at its base by a biotite–hornblende granite (Unit III granite), which forms the main mass of the Paine granite (~600–1000 m). This has been dated by Michel *et al.* (2008) at 12.49 ± 0.02 Ma, with an antecryst dated at 12.54 ± 0.03 Ma. The contacts between the Paine granite and the PMC are subhorizontal and always sharp and straight. Rarely, fine-grained decimetre-scale monzodioritic enclaves, with chilled margins, are found in the granite. Large rounded (metre to decimetre in scale) granodioritic enclaves also occur. Only a few granitic rocks are exposed beneath the mafic complex. At the base of Co. Castillo (Fig. 2) a biotite–hornblende granite similar to the Unit III granite is in contact with the lowermost part of the mafic complex. This is cross-cut by an aplite and a mafic dike, with no extension in the overlying mafic rocks, suggesting that this granite

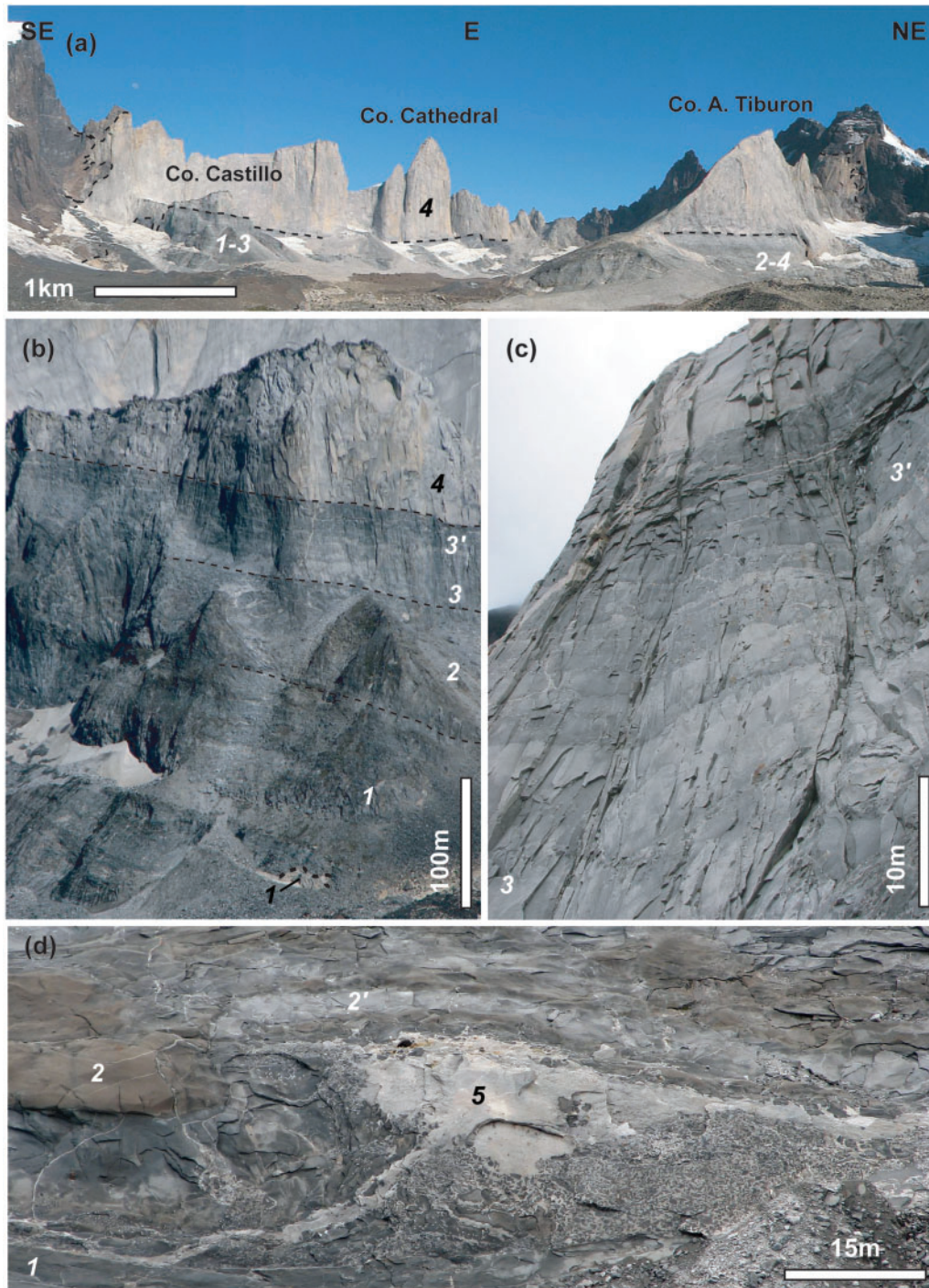


Fig. 4. Field photographs of the TPIC laccolith. (a) The mafic rocks form a concave-upward bowl in the central part of the laccolith in the Valle Frances. Names of summits are indicated on the map in Fig. 1. (b) Photograph of the Co. Castillo that clearly shows the layered nature of the mafic unit, as well as the sharp contact between the mafic and granite rocks overlying them. Three mafic units are distinguished based on field and geochemical data: a lower hornblende-gabbro, an upper hornblende-gabbro and a larger accumulation of monzodioritic sills at the top of the section. Boundaries between the units are indicated by dashed lines. Dioritic sills occur in the lower hornblende-gabbro unit and less frequently in the upper hornblende-gabbro. Diorite-gabbro contacts show evidence of ductile deformation. Each hornblende-gabbro unit is built up of multiple 10–50 m thick sills. (c) The uppermost monzodiorite unit is built up of a succession of metre-thick monzodioritic sills, clearly visible in this photograph of the top of Co. Castillo. (d) Photograph of the western side of Co. Aleta de Tiburon. Monzodioritic enclaves have accumulated at the border of a porphyritic granite pod, emplaced at the contact between the lower and upper hornblende-gabbro. A succession of dark olivine-bearing and light grey olivine-free gabbros is visible at the top of the photograph. 1, Lower hornblende-gabbro; 2, upper hornblende-gabbro; 3, layered monzodiorite and 3', monzodiorite enclave in enclave-rich porphyritic granite; 4, granite; 5, enclave-rich porphyritic granite.

crystallized prior to the lower hornblende-gabbro. The described mafic dikes display a mingled rim with the surrounding granite.

(7) *Porphyritic granite*

The mafic sheets are commonly back-veined by sills and dikes of more felsic composition, which are collectively referred to as porphyritic granites. They are often quartz-bearing and contain alkali feldspar phenocrysts. Felsic sills and dikes typically contain enclaves (20–50%), which form swarms along the border of the dikes (Fig. 4d). Most enclaves are dioritic, display discrete chilled margins, and are sometimes dismembered and fractured, with mingling textures at the contact between the enclave core and the surrounding porphyritic granite. These dioritic enclaves are identical to the elongated enclaves found in the uppermost level of the monzodiorite unit. Some of the enclaves in the porphyritic granite have granodioritic compositions. They are similar to the mafic enclaves that occur at base of the granite. These late-stage porphyritic granite intrusions often form lens-shaped bodies of ~50 m × 10 m in the laccolith. They are connected to a number of small-scale (<1 m) diapirs of (grano-)dioritic composition, intruding the overlying mafic sheets. Most of the diapirs are cylindrical features less than 20 cm in diameter. Internal layering is common and the core is characterized by miarolitic cavities with centimetre-scale crystals of quartz, feldspar and titanite.

All the plutonic rocks of the laccolith are intruded by mafic, granitic, aplitic and composite mafic–felsic dikes. Below, the PMC rocks of the feeder zone and the laccolith are considered separately.

PETROGRAPHY OF THE PAINE MAFIC COMPLEX (PMC) ROCKS

Feeder zone (FZ) gabbro-norites

The layering in the FZ layered gabbro-norite is expressed by alternating plagioclase-rich (leucocratic anorthosite to pyroxene–hornblende gabbro-norite) and pyroxene-rich (mesocratic gabbro-norite to pyroxene–hornblende gabbro-norite) centimetre-thick bands. Crystals display no evidence of substantial sub-solidus deformation. Anhedronal olivine and euhedral plagioclase (An_{70–65}) occur as inclusions in poikilitic ortho- and clinopyroxene, which are co-crystallizing with ilmenite. Brown hornblende partially replaces pyroxene and shows late interstitial growth, together with biotite and intercumulus plagioclase (An_{60–50}). Biotite and hornblende abundance may vary from one sample to another, from about 3 to rarely 20 vol. %. Pyrite is also present.

Rocks of the FZ pyroxene–hornblende gabbro-norite unit display anhedronal olivine and pyroxene inclusions in brown hornblende, and euhedral plagioclase. The crystallization

order is the same as in the layered gabbro-norite. Hornblende represents up to about 40% of the modal mineralogy. Plagioclase frequently displays anhedral, reversely zoned cores. Oxides and sulfides (magnetite, ilmenite and pyrite) are found as inclusions in hornblende cores and within the groundmass. Apatite is also observed.

Laccolith (LA) hornblende-gabbros

Two features of the lower hornblende-gabbros are different from those of all the other hornblende-gabbros of the PMC: (1) the hornblende contains no plagioclase inclusions; (2) the anhedral brown hornblende cores are rimmed by biotite. The observed hornblende and plagioclase microtextures may reflect a different crystallization sequence, or a variation in nucleation and growth rates (e.g. Vernon, 2004). As in other TPIC hornblende-gabbros, olivine and clinopyroxene are found as inclusions in hornblende cores. Olivine also occurs as inclusions in orthopyroxene in the most mafic samples from the upper hornblende-gabbro. The groundmass of these gabbros is composed of biotite, green hornblende, plagioclase, apatite and minor quartz, magnetite, ilmenite, titanite, pyrite and K-feldspar. On average, the lower hornblende-gabbro has higher modal biotite and apatite than the other Paine hornblende-gabbros. The vertical sections of Co. Aleta de Tiburon and Co. Castillo show a progressive transition (bottom to top) from olivine- and pyroxene-bearing porphyritic hornblende-gabbro, towards an olivine-free hornblende-gabbro, followed by fine-grained monzodiorite. Locally, granodiorite, with quartz and alkali-feldspar phenocrysts, is also observed along the sill margins.

The LA upper hornblende-gabbro is petrographically very similar to the feeder-zone pyroxene–hornblende gabbro-norite. However, the groundmass is modally more important and generally more felsic, with green hornblende, plagioclase, apatite, ilmenite, titanite, and rare biotite and pyrite.

Monzodiorites (feeder zone and laccolith)

The mineralogy of the monzodiorites is similar to that of the groundmass of the LA hornblende-gabbros, with millimetre-sized crystals of plagioclase, biotite, green hornblende, apatite and minor quartz, magnetite and ilmenite and rare K-feldspar. Biotite is the most abundant ferro-magnesian phase. Titanite is typically a minor phase.

Dikes (feeder zone and laccolith)

A variety of post-plutonic mafic dikes are found in the TPIC area. All samples have a hornblende + plagioclase ± biotite groundmass and some of them are olivine-phyric (08JL407) or hornblende-phyric (07JL152). The hornblende macrocrysts of the latter display an anhedral core rimmed by biotite and subsequent hornblende crystallization, whose composition is similar to that of the microcrystals in the groundmass. The most primitive dike

was found in the feeder zone area: an olivine-bearing dike (08JL407) has subhedral olivine (Fo85) macrocrysts, and euhedral plagioclase (An70–65) and clinopyroxene macrocrysts. Olivine is absent in the plagioclase–hornblende microcrystalline groundmass. Microscopic Cr-rich spinel inclusions occur in olivine.

SAMPLE LOCATIONS AND ANALYTICAL METHODS

Details of the sample locations for this study are provided as Supplementary Data Electronic Appendices 1–4, which are available for downloading at <http://www.petrology.oxfordjournals.org>.

The bulk-rock major, minor and trace element compositions of 84 PMC samples, including 15 mafic dikes, were analysed (Table 1). Almost all samples were powdered using an agate mill; some samples were powdered using a tungsten carbide mill. Dried powders (1.2 g), mixed with 6 g of lithium tetraborate, were melted at 1200°C for 3.5 min and quenched to obtain glass beads. These were used for major element determination by X-ray fluorescence (XRF) at the Institute of Mineralogy and Geochemistry, University of Lausanne, using a Philips PW 2400 spectrometer. The BHVO-1, NIMN, GA and SY-2 standards were used for quality control. Concentrations of trace elements were determined by laser ablation inductively coupled plasma mass spectrometry (LA-ICP-MS) on glass beads at the Institute of Mineralogy and Geochemistry, University of Lausanne, using a 193 nm excimer laser system (Geolas[®]) with a Perkin-Elmer ELAN 6100 DRC ICP-MS system. Operating conditions of the laser were 10 Hz frequency, 140 mJ energy and 120 µm spot size. CaO contents previously determined by XRF on the glass beads were used for internal standardization by reference to an SRM612 NIST external standard. Raw data were reduced off-line using the LAMTRACE software (Jackson *et al.*, 1992; Longrich *et al.*, 1996; Jackson, 2008a, 2008b).

Radiogenic isotopes were determined on 17 bulk-rock powders from the PMC and 10 from the Paine granite (Table 2). Whole-rock samples were analyzed for their Pb, Sr and Nd isotopic compositions at the Department of Mineralogy at the University of Geneva following the method described by Chiaradia (2009), using a Thermo TRITON mass spectrometer on Faraday cups in static mode. Pb was loaded on Re filaments using the silica gel technique and all samples (and standards) were measured at a pyrometer-controlled temperature of 1220°C. Pb isotope ratios were corrected for instrumental fractionation by a factor of 0.07% per a.m.u. based on more than 90 measurements of the SRM981 standard and using the standard values of Todt *et al.* (1996). External reproducibility of the standard ratios are 0.08% for ²⁰⁶Pb/²⁰⁴Pb,

0.11% for ²⁰⁷Pb/²⁰⁴Pb and 0.15% for ²⁰⁸Pb/²⁰⁴Pb. Sr was loaded on single Re filaments with a Ta oxide solution and measured at a pyrometer-controlled temperature of 1480°C in static mode using the virtual amplifier design to cancel out biases in gain calibration among amplifiers. ⁸⁷Sr/⁸⁶Sr values were internally corrected for fractionation using a ⁸⁸Sr/⁸⁶Sr value of 8.375209. Raw values were further corrected for external fractionation by a value of +0.03‰, determined by repeated measurements of the SRM987 standard (⁸⁷Sr/⁸⁶Sr = 0.710250). External reproducibility of the ⁸⁷Sr/⁸⁶Sr ratio for the SRM987 standard is 7 µg g⁻¹ (1σ). Nd was loaded on double Re filaments with 1 M HNO₃ and measured in static mode with the virtual amplifier design. ¹⁴³Nd/¹⁴⁴Nd values were internally corrected for fractionation using a ¹⁴⁶Nd/¹⁴⁴Nd value of 0.7219 and the ¹⁴⁴Sm interference on ¹⁴⁴Nd was monitored on the mass ¹⁴⁷Sm and corrected by using a ¹⁴⁴Sm/¹⁴⁷Sm value of 0.206700. External reproducibility of the JNdi-1 standard (Tanaka *et al.*, 2000) is <5 µg g⁻¹ (1σ). ⁸⁷Sr/⁸⁶Sr and ¹⁴³Nd/¹⁴⁴Nd whole-rock compositions were corrected for time-integrated decay of ⁸⁷Rb and ¹⁴⁷Sm using Rb, Sr, Sm and Nd concentrations determined by LA-ICP-MS on bulk-rocks and an age of 12.5 Ma. The resulting time-integrated corrections are small (~0.002%).

GEOCHEMISTRY OF THE TORRES DEL PAINE INTRUSIVE COMPLEX (TPIC)

The rocks of the PMC (comprising mafic rocks from the feeder zone and laccolith) span a range of compositions from calc-alkaline, through high-K calc-alkaline to shoshonitic (Table 1, Fig. 5a and b) and are all metaluminous (Fig. 5c). The Paine granitic rocks are metaluminous to peraluminous and belong to the high-K calc-alkaline series. The gabbroic rocks display a large scatter in the Harker plots of Al₂O₃, FeO, CaO and K₂O versus SiO₂ (Fig. 6) and Ba, Sc, Sr and Nd versus SiO₂ (Fig. 7). The chemical evolution from monzodiorite to granite defines clear trends, which are sometimes kinked (e.g. Al₂O₃, Na₂O, P₂O₅, Ba, Zr, REE) and sometimes straight (e.g. CaO, FeO, K₂O, Th, Rb). The kinks are controlled by the appearance of new mineral phases, which changes the bulk partition coefficients. Incompatible element ratios, such as Th/Rb, show no trend considering all TPIC samples; the ratios Nb/La, Th/La, Nb/Th, La/Sm, Sm/Yb, La/Ta, Nb/Ta and Zr/Hf also show no trend in the PMC samples proper.

Trace element patterns normalized to primitive mantle values (Sun & McDonough, 1989) and chondrite-normalized rare earth element (REE) patterns (Boynton, 1984) are presented in Fig. 8. Overall, the TPIC rocks show only moderate variations between the most primitive gabbros and granitic rocks, spanning a range from 20 to 250 µg g⁻¹ for Rb and from 2 to 20 µg g⁻¹ for Y (Table 1;

Table 1: Bulk-rock major and trace element data for the Torres del Paine mafic complex

	FZ layered gabbronorite						FZ Px-Hbl-gabbronorite							
	5JM10*	8JL415	8JL422	8JL430	8JL435	8JL449	4JM35*	4JM36*	4JM37*	5JM4	5JM9*	8JL428	8JL445	8JL450
<i>Major elements (wt %)</i>														
SiO ₂	49.75	50.59	52.57	51.85	48.68	49.20	46.28	47.90	48.63	47.93	46.84	45.61	45.74	46.78
TiO ₂	2.52	1.05	0.93	2.42	1.58	1.98	1.92	1.48	2.55	1.22	1.62	1.35	3.96	1.87
Al ₂ O ₃	17.11	13.83	13.80	16.76	22.75	21.71	15.63	15.88	18.88	14.30	16.07	14.98	15.48	16.23
Fe ₂ O ₃	10.40	15.60	11.10	10.64	7.18	6.64	12.08	11.83	9.21	13.53	11.80	14.23	13.40	11.69
MnO	0.19	0.31	0.19	0.20	0.10	0.09	0.17	0.18	0.13	0.18	0.17	0.19	0.18	0.17
MgO	6.47	9.42	10.48	5.78	4.62	4.25	11.17	9.88	5.61	10.81	9.07	10.45	9.41	10.62
CaO	8.35	6.51	7.56	7.89	11.67	10.29	7.78	7.51	9.23	8.11	10.09	8.48	8.42	7.91
Na ₂ O	2.84	1.85	1.91	2.60	2.38	3.50	2.40	2.51	3.31	2.30	2.56	1.90	2.30	2.33
K ₂ O	0.71	0.48	0.83	0.96	0.51	0.89	1.26	1.45	1.23	0.73	0.55	0.68	0.66	1.07
P ₂ O ₅	0.51	0.44	0.11	0.56	0.11	0.29	0.34	0.29	0.41	0.19	0.35	0.26	0.24	0.38
LOI	0.54	-0.07	0.54	0.43	0.26	0.77	0.82	0.98	0.49	0.45	0.50	1.46	0.16	0.85
Total	99.41	100.08	100.08	100.11	99.85	99.63	99.88	99.87	99.68	99.80	99.67	99.71	99.96	99.94
Mg#	55.21	54.46	65.15	51.86	56.02	55.90	64.68	62.33	54.71	61.28	60.35	59.28	58.20	64.28
<i>Trace elements ($\mu\text{g g}^{-1}$)</i>														
Ni	33.2	121.8	89.3	33.0	14.4	66.1	148.7	78.3	31.0	86.0	94.5	623.5	74.1	127.0
V	332	230	177	270	190	207	155	153	216	136	253	123	301	145
Cr	142	282	315	107	40	83	210	221	198	227	251	245	86	117
Co	59.9	54.1	56.3	39.7	28.8	29.5	82.8	74.1	50.2	68.2	108.6	110.8	64.8	59.3
Sc	27.1	28.4	28.1	26.3	18.5	23.5	18.1	17.6	18.3	23.3	28.1	22.3	25.2	17.0
Cs	1.76	0.79	1.52	1.72	0.48	0.81	1.79	3.86	1.10	0.74	0.46	1.60	0.95	1.23
Rb	20.0	14.3	24.1	28.1	11.6	14.7	21.2	33.4	24.3	14.6	11.1	16.5	12.7	19.0
Ba	184	141	183	258	150	224	213	222	248	157	162	156	171	213
Th	2.03	2.02	2.70	3.27	1.17	1.99	2.46	3.76	2.67	2.09	2.27	2.17	1.87	2.41
U	0.53	0.56	0.71	1.06	0.28	0.59	0.66	1.08	0.62	0.71	0.53	0.66	0.50	0.71
Nb	15.3	6.6	8.2	n.a.	7.8	16.8	16.1	13.9	20.3	10.1	11.6	8.9	19.8	15.1
Ta	1.46	0.48	0.53	n.a.	0.52	1.00	2.20	1.31	2.14	0.60	1.62	0.57	1.20	0.97
La	16.2	13.0	11.7	22.3	8.1	16.8	15.6	17.9	18.7	12.4	14.1	11.2	12.5	15.6
Ce	32.8	27.7	23.9	44.4	16.3	37.6	32.5	37.1	37.9	26.1	30.0	24.3	26.3	32.3
Pb	5.42	3.66	4.51	8.20	2.79	10.22	5.97	6.46	15.56	3.31	3.03	3.92	3.37	5.49
Pr	3.62	3.37	2.79	4.84	1.86	4.79	3.76	4.32	4.32	3.07	3.50	2.90	3.12	3.73
Sr	604	454	411	605	747	967	673	650	810	496	714	608	641	701
Nd	15.7	14.2	11.4	20.1	7.8	21.0	15.6	19.6	19.1	12.9	15.3	12.6	13.3	15.7
Hf	1.60	0.86	1.67	2.16	0.94	2.26	2.46	2.72	2.47	1.77	1.46	1.48	1.83	2.26
Zr	67	34	65	98	35	88	107	108	107	70	64	58	80	95
Sm	3.42	2.95	2.51	4.41	1.78	4.70	3.30	4.43	3.99	2.77	3.18	2.73	2.83	3.06
Eu	1.58	1.22	0.92	1.56	1.08	1.77	1.22	1.35	1.38	1.10	1.44	0.98	1.13	1.19
Gd	2.92	2.98	2.36	4.61	1.56	4.46	3.13	3.86	2.84	2.82	3.37	2.55	2.59	2.89
Tb	0.402	0.386	0.373	0.608	0.240	0.633	0.417	0.546	0.396	0.406	0.472	0.350	0.360	0.389
Y	13.2	13.0	12.1	20.8	7.1	18.7	13.2	16.1	13.5	13.0	13.5	10.6	10.7	11.8
Dy	2.65	2.52	2.35	3.36	1.48	3.91	2.53	3.03	2.70	2.43	2.83	2.23	2.30	2.31
Ho	0.464	0.473	0.453	0.607	0.266	0.703	0.481	0.538	0.402	0.468	0.545	0.406	0.396	0.447
Er	1.28	1.31	1.25	1.70	0.75	1.94	1.30	1.43	1.28	1.23	1.37	1.04	1.12	1.15
Tm	0.180	0.198	0.182	0.298	0.101	0.263	0.183	0.237	0.184	0.170	0.198	0.144	0.149	0.169
Yb	1.25	1.44	1.35	1.83	0.60	1.57	1.06	1.45	1.15	1.21	1.14	0.95	1.05	1.00
Lu	0.145	0.214	0.184	0.252	0.106	0.230	0.157	0.223	0.172	0.178	0.170	0.127	0.151	0.138

(continued)

Table 1: Continued

	FZ layered gabbro						FZ Px-Hbl-gabbro											
	5JM10*	8JL415	8JL422	8JL430	8JL435	8JL449	4JM35*	4JM36*	4JM37*	5JM4	5JM9*	8JL428	8JL445	8JL450				
Be	1.22	1.54	1.35	2.17	1.74	1.80	1.35	n.a.	n.a.	1.31	2.37	1.36	1.45	1.86				
Cu	23.8	30.9	36.8	27.8	10.6	32.8	31.7	n.a.	n.a.	46.6	46.5	404.6	50.9	28.4				
Zn	91.8	133.5	91.8	77.4	62.8	70.4	83.5	97.6	73.3	82.6	75.3	99.4	106.9	94.8				
Ga	29.5	19.7	21.3	26.1	26.9	30.2	27.5	19.0	22.0	22.2	26.0	19.9	22.2	23.8				
Laccolith lower Hbl-gabbro																		
	7JL9	7JL10	7JL98	7JL99	7JL101	7JL107	7JL108	7JL116	7JL149	7JL150	7JL154	7JL156	8JL370	8JL372	8JL375	8JL381	8JL382	8JL384
<i>Major elements (wt %)</i>																		
SiO ₂	49.61	47.23	45.57	48.32	46.55	50.30	46.16	45.90	46.86	47.05	48.21	48.64	48.56	46.92	49.37	48.90	46.59	48.16
TiO ₂	2.22	2.29	2.24	1.98	2.02	1.71	1.37	1.53	1.30	1.86	2.09	1.88	2.00	1.36	1.82	1.99	2.19	2.18
Al ₂ O ₃	16.02	15.39	16.03	15.95	14.80	15.32	12.72	12.87	10.74	14.87	15.89	14.28	17.07	12.69	16.98	16.01	15.23	14.70
Fe ₂ O ₃	11.36	12.57	12.98	10.85	11.32	9.50	11.08	11.07	11.87	11.14	10.82	11.40	9.84	10.70	9.97	10.33	11.71	11.54
MnO	0.16	0.19	0.20	0.16	0.19	0.15	0.20	0.17	0.18	0.18	0.16	0.20	0.16	0.16	0.16	0.16	0.17	0.19
MgO	6.59	8.23	6.64	7.27	9.27	7.28	13.88	14.09	17.08	9.74	7.30	9.70	4.83	14.23	5.15	7.19	8.77	8.55
CaO	6.09	6.32	7.36	7.91	9.18	7.83	7.83	8.58	5.88	8.00	8.01	6.28	9.64	7.66	9.49	7.61	8.08	7.20
Na ₂ O	4.09	3.37	3.64	3.77	2.77	3.76	2.05	2.37	2.25	3.13	3.67	3.52	3.78	1.89	3.42	3.40	3.26	3.40
K ₂ O	2.16	2.45	2.51	1.72	1.91	2.20	2.30	1.20	1.52	2.05	2.10	2.38	1.55	1.97	1.42	2.24	1.68	2.21
P ₂ O ₅	0.62	0.57	1.13	0.54	0.50	0.72	0.39	0.47	0.43	0.48	0.56	0.61	0.68	0.41	0.54	0.56	0.72	0.58
LOI	0.67	0.78	0.92	1.20	1.14	0.76	1.69	1.62	1.27	1.20	0.82	0.90	1.06	1.49	0.97	1.24	1.20	1.02
Total	99.59	99.42	99.23	99.69	99.72	99.60	99.81	100.04	99.61	99.78	99.67	99.86	99.17	99.65	99.31	99.68	99.66	99.79
Mg#	53.45	56.48	50.33	57.04	61.87	60.31	71.28	71.60	74.03	63.39	57.20	62.78	49.28	72.50	50.57	57.96	59.75	59.48
<i>Trace elements ($\mu\text{g g}^{-1}$)</i>																		
Ni	74.0	90.1	61.4	104.6	155.2	121.2	315.8	376.4	458.9	160.4	103.0	150.3	29.4	354.2	31.9	106.0	109.2	120.0
V	170	190	200	192	211	175	189	208	171	189	199	158	214	185	238	181	222	176
Cr	117	143	101	98	366	295	845	891	1193	461	286	326	73	840	97	223	235	269
Co	40.3	47.3	36.1	43.4	46.1	33.4	55.3	57.8	68.4	42.0	35.9	43.4	27.4	56.6	28.3	37.0	44.2	41.9
Sc	15.2	16.3	16.1	22.4	26.3	21.3	23.9	26.8	20.1	22.7	22.3	17.6	26.7	24.7	29.8	21.3	23.4	19.1
Cs	2.01	6.00	6.89	1.76	3.56	2.71	13.18	2.89	2.28	4.03	2.58	3.13	2.70	2.75	1.65	3.60	2.04	6.19
Rb	42.7	76.3	71.0	32.8	43.5	66.3	79.0	22.6	35.9	37.4	41.5	44.8	39.0	43.5	30.5	55.7	28.7	43.2
Ba	504	483	503	428	336	357	302	337	279	434	474	473	329	310	330	440	395	463
Th	7.21	6.03	6.41	5.28	3.66	7.25	3.58	3.98	4.75	4.71	5.08	6.69	4.63	4.22	5.67	5.56	6.28	7.46
U	1.71	1.84	1.94	1.55	0.98	2.46	1.19	1.00	1.24	1.31	1.24	1.49	1.36	1.18	2.05	1.45	1.37	1.45
Nb	32.7	31.0	39.9	29.4	23.6	33.3	18.2	20.9	18.1	25.0	29.0	30.4	28.0	18.8	21.2	28.4	26.0	31.5
Ta	1.93	1.78	2.15	1.66	1.29	1.87	0.99	1.15	1.03	1.44	1.55	1.64	1.49	1.01	1.25	1.66	1.41	1.70
La	42.5	37.2	46.3	35.8	33.7	43.3	23.0	27.9	24.5	28.8	35.8	40.5	35.2	25.7	31.0	35.6	37.4	49.4
Ce	81.8	73.2	91.4	68.7	63.8	80.4	46.6	55.4	48.4	58.5	70.9	80.4	70.1	51.4	60.6	71.1	76.4	91.0
Pb	5.72	5.19	4.68	5.66	4.03	5.46	5.15	4.98	5.50	9.94	6.73	10.88	3.98	4.12	6.41	7.97	7.03	8.92
Pr	8.98	8.19	10.41	7.60	7.02	8.80	5.28	6.59	5.50	6.96	7.92	9.15	7.92	5.97	6.82	8.04	8.91	10.33
Sr	914	872	1027	736	611	814	493	550	413	706	797	782	806	491	680	735	836	750
Nd	35.3	33.8	40.0	30.6	28.2	34.2	20.7	25.2	21.8	28.1	31.6	33.9	31.8	23.3	27.5	31.1	35.3	40.0
Hf	4.38	4.27	4.78	4.38	3.09	4.10	2.71	2.74	2.83	3.55	3.86	3.82	3.60	2.43	3.32	3.75	3.90	4.15
Zr	208	197	221	198	144	177	112	125	116	159	173	180	178	96	150	168	177	175
Sm	6.50	6.65	7.39	6.28	5.30	6.15	4.45	4.84	4.34	5.41	6.11	6.54	6.31	4.57	5.53	5.93	6.96	7.60

(continued)

Table 1: Continued

Laccolith lower Hbl-gabbro																		
	7JL9	7JL10	7JL98	7JL99	7JL101	7JL107	7JL108	7JL116	7JL149	7JL150	7JL154	7JL156	8JL370	8JL372	8JL375	8JL381	8JL382	8JL384
Eu	2.02	2.00	2.20	1.75	1.69	1.93	1.27	1.61	1.27	1.74	1.96	1.86	2.03	1.37	1.71	1.93	2.10	2.12
Gd	5.52	5.23	6.31	5.62	4.87	5.31	4.00	4.61	4.10	4.96	5.27	5.28	5.51	4.32	5.18	5.19	5.74	6.72
Tb	0.663	0.745	0.859	0.762	0.667	0.733	0.560	0.605	0.577	0.668	0.731	0.692	0.820	0.641	0.743	0.703	0.798	0.855
Y	23.3	22.6	26.7	33.2	21.0	23.2	18.5	18.4	18.1	20.3	23.3	23.6	24.6	18.5	23.8	21.9	23.2	26.4
Dy	4.63	4.59	5.17	4.52	4.13	4.59	3.55	3.65	3.48	3.99	4.26	4.17	4.90	3.61	4.73	4.31	4.77	5.39
Ho	0.901	0.820	0.948	0.863	0.771	0.849	0.700	0.746	0.687	0.720	0.858	0.802	0.956	0.697	0.954	0.806	0.893	1.000
Er	2.37	2.26	2.44	2.24	2.00	2.42	1.96	1.82	1.81	2.13	2.19	2.14	2.56	1.93	2.54	2.09	2.42	2.61
Tm	0.316	0.318	0.336	0.310	0.280	0.341	0.276	0.277	0.252	0.289	0.290	0.311	0.364	0.280	0.370	0.293	0.321	0.355
Yb	2.02	2.13	2.33	2.03	1.86	2.22	1.69	1.70	1.81	1.89	1.94	1.93	2.51	1.92	2.34	1.99	2.00	2.39
Lu	0.283	0.311	0.337	0.284	0.260	0.333	0.255	0.253	0.258	0.265	0.284	0.280	0.341	0.267	0.341	0.288	0.302	0.351
Be	2.78	1.85	2.30	2.27	2.14	2.66	2.22	2.37	1.69	2.70	2.10	2.68	2.28	1.69	1.90	2.45	2.71	2.51
Cu	29.6	23.2	10.6	36.4	35.6	40.5	24.7	45.1	50.2	50.4	31.2	23.7	13.7	36.2	31.0	22.1	42.6	20.8
Zn	65.3	76.7	88.0	10.4	662.5	57.3	531.3	109.4	520.8	425.7	285.5	15.3	81.1	80.3	93.6	104.8	87.6	106.3
Ga	31.4	30.4	41.7	38.7	33.2	34.4	28.3	37.1	32.8	46.1	38.4	37.4	34.2	30.1	33.3	39.6	35.6	38.7
Laccolith upper Hbl-gabbro																		
	05JM18*	05JM29*	07JL158	07JL160	07JL161	07JL162	07JL163	07JL164G	08JL386	08JL388	08JL389							
<i>Major elements (wt %)</i>																		
SiO ₂	51.12	48.02	45.96	50.59	50.81	48.69	53.18	50.58	48.35	46.58	51.73							
TiO ₂	1.66	1.36	1.30	1.75	1.35	1.40	1.36	1.32	1.69	1.64	1.72							
Al ₂ O ₃	16.05	14.56	12.11	15.92	17.53	13.47	16.64	15.85	14.80	13.38	16.53							
Fe ₂ O ₃	9.49	9.81	11.89	9.77	8.63	11.33	8.71	9.26	10.29	11.62	10.08							
MnO	0.14	0.15	0.17	0.15	0.13	0.17	0.14	0.14	0.16	0.17	0.16							
MgO	5.77	9.93	15.79	6.46	6.19	11.52	5.20	8.47	9.69	12.69	5.41							
CaO	9.13	8.50	7.45	8.75	9.77	7.42	8.41	9.05	8.61	8.45	8.25							
Na ₂ O	3.39	3.09	2.34	3.61	3.51	2.97	3.80	3.42	3.07	2.38	3.48							
K ₂ O	1.32	1.16	1.01	1.21	1.00	1.03	1.38	0.93	1.30	1.00	1.56							
P ₂ O ₅	0.39	0.41	0.36	0.40	0.30	0.35	0.36	0.33	0.52	0.51	0.45							
LOI	0.80	1.14	0.94	0.54	0.49	1.13	0.51	0.66	1.08	1.21	0.70							
Total	99.31	98.23	99.49	99.20	99.76	99.58	99.72	100.10	99.64	99.75	100.10							
Mg#	54.65	66.72	72.46	56.73	58.70	66.82	54.21	64.45	65.12	68.40	51.54							
<i>Trace elements (µg g⁻¹)</i>																		
Ni	50.5	199.77	427.7	86.8	75.9	256.3	51.1	172.6	219.4	331.6	61.0							
V	202	173.64	147	193	169	159	160	153	195	219	191							
Cr	267	573.70	941	268	259	600	157	412	422	662	188							
Co	66.2	67.34	66.4	32.3	30.1	55.0	29.5	41.4	43.7	59.3	32.3							
Sc	26.4	24.95	22.0	24.4	25.1	21.9	22.6	23.9	24.7	26.8	24.7							
Cs	2.05	2.70	1.79	1.66	1.91	2.89	2.85	2.04	1.07	2.20	3.82							
Rb	35.3	26.52	21.6	28.8	24.1	26.5	33.2	23.0	24.8	23.2	46.4							
Ba	309	312.24	251	301	251	250	290	251	327	255	330							
Th	5.35	4.00	3.03	3.65	3.17	4.63	5.66	3.09	4.17	4.30	4.54							
U	1.95	1.21	0.81	1.01	0.83	1.29	1.60	0.84	1.07	1.14	1.83							
Nb	18.3	18.74	15.6	18.6	14.2	16.1	14.9	14.1	22.4	17.2	19.6							
Ta	2.03	n.a.	0.87	1.04	0.79	0.87	0.85	0.79	1.31	0.95	1.12							
La	24.8	26.09	20.0	21.6	18.2	21.5	25.9	21.4	29.4	24.4	29.5							

(continued)

Table 1: Continued

Laccolith upper Hbl-gabbro											
	05JM18*	05JM29*	07JL158	07JL160	07JL161	07JL162	07JL163	07JL164G	08JL386	08JL388	08JL389
Ce	48.4	51.95	40.1	45.8	37.7	43.1	49.6	42.5	59.2	52.2	58.1
Pb	4.79	5.27	3.07	4.84	6.05	12.02	26.79	9.60	4.51	3.34	17.22
Pr	5.76	5.87	4.69	5.34	4.51	4.98	5.39	4.65	6.85	6.33	6.68
Sr	613	637.07	499	570	610	473	545	566	696	574	570
Nd	23.1	25.20	19.3	21.9	19.2	20.1	21.5	19.6	28.7	27.3	26.7
Hf	3.50	3.41	2.44	3.37	2.71	2.86	3.29	2.65	3.41	2.55	3.51
Zr	145	142.03	105	140	104	126	136	105	151	91	145
Sm	5.41	5.19	3.71	4.74	3.90	4.32	4.25	4.04	5.58	6.02	6.18
Eu	1.53	1.67	1.23	1.60	1.37	1.26	1.34	1.33	1.88	1.79	1.82
Gd	4.84	4.65	3.50	4.75	3.95	4.19	4.12	4.05	5.28	5.62	5.80
Tb	0.684	0.64	0.511	0.686	0.580	0.577	0.576	0.621	0.740	0.810	0.803
Y	21.3	20.62	15.9	21.4	17.8	18.8	18.6	18.9	20.8	21.6	25.0
Dy	4.33	4.09	3.08	4.24	3.53	3.64	3.63	3.64	4.38	4.82	5.00
Ho	0.833	0.76	0.601	0.795	0.656	0.684	0.617	0.673	0.811	0.880	0.971
Er	2.02	2.14	1.53	2.18	1.85	1.93	1.90	1.70	2.07	2.31	2.58
Tm	0.306	0.31	0.221	0.298	0.268	0.278	0.268	0.253	0.295	0.308	0.353
Yb	2.19	1.88	1.44	1.94	1.38	1.73	1.76	1.56	1.92	2.22	2.31
Lu	0.302	0.29	0.207	0.291	0.247	0.255	0.265	0.236	0.280	0.250	0.342
Be	1.85	2.03	1.74	2.08	1.94	2.51	2.14	2.01	2.25	1.64	2.36
Cu	20.6	35.99	43.9	21.3	24.1	47.3	19.7	33.7	37.8	44.8	25.8
Zn	62.6	67.84	16.9	233.2	81.9	64.8	16.1	170.8	85.0	95.5	125.0
Ga	40.7	37.36	25.8	33.3	30.1	32.8	31.5	29.2	30.9	26.0	34.8

Feeder zone diorite								
	4JM39*	5JM6*	5JM11*	5JM12*	5JM14*	5JM17*	8JL419	8JL446
<i>Major elements (wt %)</i>								
SiO ₂	59.45	54.91	53.34	57.43	59.60	55.78	50.57	55.02
TiO ₂	1.02	1.89	1.90	1.78	1.55	1.68	2.32	2.04
Al ₂ O ₃	17.50	16.04	16.26	15.45	15.35	17.36	16.74	16.66
Fe ₂ O ₃	6.43	10.21	9.43	9.42	8.86	8.63	10.31	9.39
MnO	0.08	0.16	0.16	0.15	0.13	0.16	0.16	0.17
MgO	1.28	3.68	3.81	2.97	2.05	2.38	5.12	3.94
CaO	4.42	6.53	7.43	5.27	4.61	5.74	7.64	6.71
Na ₂ O	4.52	3.64	3.77	3.58	3.75	4.42	3.51	2.74
K ₂ O	2.13	2.00	2.14	2.33	3.03	2.19	1.71	1.98
P ₂ O ₅	0.35	0.51	0.46	0.46	0.38	0.56	0.50	0.39
LOI	1.20	0.06	0.17	0.47	0.44	0.18	1.06	0.71
Total	98.38	99.64	98.88	99.31	99.74	99.09	99.66	99.75
Mg#	28.35	41.70	44.47	38.41	31.45	35.32	49.62	45.40
<i>Trace elements (µg g⁻¹)</i>								
Ni	6.5	10.3	10.2	6.8	7.1	4.1	33.2	14.5
V	94	171	209	210	152	95	198	222
Cr	88	58	85	58	46	29	65	31
Co	42.1	56.0	46.2	59.3	53.6	45.8	32.3	27.1
Sc	15.2	24.4	25.3	22.1	20.2	22.3	23.5	23.6

(continued)

Table 1: Continued

Feeder zone diorite																		
	4JM39*	5JM6*	5JM11*	5JM12*	5JM14*	5JM17*	8JL419	8JL446										
Cs	3.79	1.93	1.67	3.77	4.96	2.55	1.47	2.32										
Rb	64.3	61.2	59.5	72.0	92.5	64.8	34.5	56.9										
Ba	593	524	708	446	588	696	382	567										
Th	8.22	5.68	6.04	7.99	12.01	8.69	4.88	5.60										
U	1.61	1.96	1.85	1.85	1.53	1.67	1.19	1.35										
Nb	25.3	31.1	33.4	23.8	23.9	43.1	25.2	19.9										
Ta	3.77	2.87	2.62	2.91	2.85	3.35	1.51	1.29										
La	32.9	43.2	40.1	35.3	47.5	56.6	29.6	27.4										
Ce	67.4	88.6	79.4	71.4	93.1	119.8	59.9	59.7										
Pb	18.32	10.19	8.47	29.15	16.94	14.70	18.56	30.70										
Pr	7.42	10.48	8.95	7.99	10.46	13.56	6.99	6.83										
Sr	482	507	551	409	316	767	655	539										
Nd	30.1	41.5	36.5	34.6	43.8	57.7	28.1	27.8										
Hf	7.55	5.15	5.98	5.76	7.44	5.69	4.11	4.91										
Zr	367	226	264	235	300	231	180	195										
Sm	5.76	8.25	7.58	6.94	9.30	11.40	5.72	5.72										
Eu	1.99	2.21	2.08	1.99	1.76	2.84	1.74	1.81										
Gd	5.08	7.67	6.92	6.98	7.74	9.56	5.12	4.95										
Tb	0.723	1.082	0.911	0.962	1.194	1.252	0.694	0.777										
Y	24.7	34.9	31.3	33.7	39.9	42.0	21.0	23.8										
Dy	4.35	6.82	6.34	6.30	7.50	8.02	4.24	4.63										
Ho	0.864	1.209	1.222	1.225	1.462	1.540	0.756	0.841										
Er	2.40	3.56	3.23	3.46	4.06	4.07	2.10	2.41										
Tm	0.387	0.517	0.394	0.472	0.603	0.608	0.289	0.390										
Yb	2.44	3.10	3.24	3.22	3.81	3.32	1.88	2.24										
Lu	0.387	0.435	0.421	0.447	0.539	0.512	0.269	0.342										
Be	2.00	2.55	2.52	3.06	4.87	2.70	2.34	2.04										
Cu	9.2	14.7	291.0	17.9	9.1	12.7	20.2	19.1										
Zn	n.a.	91.2	83.7	121.3	98.5	97.4	113.7	138.6										
Ga	61.7	59.9	74.8	51.6	65.5	74.9	36.6	44.7										
Laccolith diorite																		
	4JM82*	4JM84	5JM33	5JM36*	7JL20	7JL50	7JL51	7JL96	7JL151	7JL157	7JL165F	7JL165G	8JL350	8JL367	8JL380	8JL385	8JL390	8JL391
<i>Major elements (wt %)</i>																		
SiO ₂	50.57	58.31	52.21	53.63	59.09	50.32	52.31	50.84	59.50	51.44	54.50	55.15	55.53	59.04	54.65	51.24	61.71	62.27
TiO ₂	2.33	1.50	1.93	2.29	1.64	1.55	1.76	2.15	1.15	2.16	1.92	1.99	1.48	1.25	2.05	2.43	1.27	1.18
Al ₂ O ₃	16.69	17.26	16.11	16.37	15.89	14.95	16.39	17.67	16.65	15.99	16.67	16.20	16.78	17.52	17.07	17.68	15.95	15.72
Fe ₂ O ₃	10.60	6.80	9.32	9.63	7.73	9.77	9.20	8.61	6.03	10.31	8.54	8.70	7.87	6.32	8.57	9.53	6.21	6.32
MnO	0.16	0.12	0.19	0.17	0.12	0.17	0.15	0.12	0.10	0.15	0.15	0.16	0.12	0.12	0.14	0.15	0.09	0.10
MgO	4.75	2.12	3.25	3.19	2.48	8.88	5.22	3.92	2.52	5.18	2.82	2.83	4.27	1.92	3.22	3.64	1.98	2.25
CaO	6.12	4.12	6.75	6.63	4.90	8.15	8.86	8.09	5.14	6.42	5.98	5.93	7.26	4.43	5.67	7.57	4.06	4.55
Na ₂ O	4.85	4.85	4.44	4.42	3.85	2.91	3.58	5.03	4.61	4.40	4.77	4.57	3.56	5.03	4.88	4.55	4.17	4.11
K ₂ O	2.16	3.15	2.42	2.51	2.82	1.85	1.36	1.13	2.68	2.35	2.63	2.86	1.92	2.96	2.52	1.95	3.38	2.71
P ₂ O ₅	0.67	0.60	0.73	0.62	0.44	0.45	0.50	0.84	0.40	0.71	0.80	0.77	0.46	0.47	0.75	0.79	0.47	0.35
LOI	0.52	0.37	0.40	0.28	0.54	1.00	0.53	1.27	0.41	0.58	0.55	0.48	0.80	0.15	0.22	0.33	0.56	0.22

(continued)

Table I: Continued

Laccolith diorite																		
	4JM82*	4JM84	5JM33	5JM36*	7JL20	7JL50	7JL51	7JL96	7JL151	7JL157	7JL165F	7JL165G	8JL350	8JL367	8JL380	8JL385	8JL390	8JL391
Total	99.46	99.21	97.75	99.75	99.50	100.09	99.90	99.66	99.18	99.70	99.33	99.63	100.07	99.21	99.74	99.85	99.85	99.78
Mg#	47.04	38.19	40.83	39.62	38.83	64.30	52.95	47.42	45.31	49.88	39.58	39.16	51.79	37.53	42.69	43.06	38.68	41.32
<i>Trace elements ($\mu\text{g g}^{-1}$)</i>																		
Ni	39.0	3.8	3.7	2.9	8.3	n.a.	n.a.	28.0	19.3	43.9	4.4	4.6	38.5	5.0	21.0	8.7	10.1	15.6
V	164	89	149	189	179	182	215	154	122	170	109	122	168	99	117	178	102	109
Cr	70	11	243	100	53	n.a.	n.a.	36	50	82	138	34	87	14	25	20	24	52
Co	52.4	12.4	21.8	58.7	16.5	n.a.	n.a.	19.6	13.2	27.3	15.0	14.7	24.0	9.1	20.3	18.4	12.4	14.3
Sc	14.7	13.6	19.1	24.9	14.7	26.0	29.9	18.0	15.3	16.8	15.3	16.8	21.0	14.0	15.7	19.0	12.6	14.3
Cs	2.00	2.96	2.14	5.17	7.63	1.51	1.03	2.04	1.94	2.89	4.07	3.88	2.56	3.74	2.52	1.96	4.29	2.58
Rb	41.2	73.6	58.4	77.1	77.8	44.7	31.8	28.9	66.4	53.4	63.4	70.7	50.9	92.0	54.3	40.2	87.4	69.6
Ba	530	577	397	460	532	346	401	270	566	503	531	522	351	669	542	509	531	457
Th	9.23	12.54	8.65	12.94	8.95	8.02	5.68	6.03	12.50	7.92	7.12	6.10	7.37	9.45	10.19	7.58	13.20	10.61
U	2.12	2.72	2.22	3.20	2.70	3.16	2.98	2.94	3.45	2.02	2.43	1.88	1.97	2.68	2.42	2.16	2.45	2.13
Nb	36.9	34.4	37.1	41.7	27.0	n.a.	n.a.	34.3	26.2	31.4	35.0	37.2	20.3	37.1	39.9	34.2	27.7	23.1
Ta	2.62	2.09	2.17	4.15	1.80	n.a.	n.a.	2.01	1.60	1.86	2.04	2.16	1.20	1.74	2.42	1.92	1.94	1.53
La	46.4	47.4	40.2	47.8	36.4	31.0	38.0	45.7	48.2	40.0	45.3	30.4	33.1	45.5	45.4	48.1	30.2	36.4
Ce	88.2	90.8	83.7	85.9	69.4	70.9	77.7	84.2	89.0	84.7	89.0	64.8	61.5	91.1	89.0	93.6	60.1	68.9
Pb	6.63	9.57	86.17	11.21	11.07	6.97	5.85	5.71	9.74	13.22	7.67	8.31	6.36	8.93	9.23	8.46	10.06	9.06
Pr	9.78	9.82	9.83	9.73	7.79	8.52	8.32	9.02	9.46	9.97	9.89	7.67	6.71	10.10	9.95	10.58	6.91	7.47
Sr	1006	696	778	708	518	618	709	1015	572	918	709	723	663	577	856	1013	495	437
Nd	38.6	36.9	38.0	43.7	29.5	29.0	29.8	36.3	34.3	38.9	39.1	32.5	26.7	39.4	39.2	41.0	27.4	28.0
Hf	5.65	5.41	4.48	5.86	4.86	3.22	3.45	4.60	5.19	4.41	4.40	1.94	3.43	6.29	5.24	4.52	5.35	3.45
Zr	261	247	204	264	195	129	176	207	208	198	207	78	151	287	250	208	233	154
Sm	7.72	6.88	7.28	8.23	5.59	5.76	6.02	6.83	6.78	7.10	7.25	7.22	5.38	7.23	7.31	7.87	5.51	5.71
Eu	2.17	1.96	2.09	2.63	1.59	1.69	1.96	2.38	1.37	2.17	2.08	2.24	1.59	1.67	2.13	2.26	1.49	1.33
Gd	6.11	5.96	6.66	9.91	5.03	5.31	6.54	5.76	5.65	6.38	6.42	6.20	4.85	6.24	6.34	6.56	5.26	4.77
Tb	0.844	0.818	0.949	1.243	0.739	0.671	0.890	0.844	0.843	0.841	0.887	0.955	0.694	0.865	0.846	0.911	0.721	0.735
Y	26.9	25.6	32.0	40.9	24.5	20.7	27.5	24.3	26.3	26.6	28.9	27.9	19.8	27.3	25.7	27.3	23.7	22.9
Dy	5.16	5.06	5.94	7.94	4.73	4.38	4.89	4.80	4.85	5.26	5.43	5.45	3.96	5.47	5.09	5.38	4.54	4.30
Ho	0.969	0.925	1.096	1.555	0.889	0.750	0.848	0.861	0.997	0.950	0.972	1.073	0.772	1.044	0.984	1.022	0.904	0.789
Er	2.67	2.49	3.05	4.21	2.30	2.20	2.41	2.41	2.71	2.77	2.93	2.64	1.89	2.74	2.55	2.60	2.32	2.35
Tm	0.377	0.387	0.445	0.640	0.347	0.320	0.389	0.345	0.380	0.359	0.372	0.368	0.266	0.378	0.368	0.395	0.357	0.302
Yb	2.37	2.50	3.03	3.78	2.35	1.94	2.44	2.04	2.39	2.35	2.38	2.37	1.90	2.54	2.42	2.44	2.41	2.30
Lu	0.370	0.365	0.413	0.590	0.335	0.283	0.344	0.293	0.351	0.339	0.386	0.332	0.259	0.378	0.369	0.353	0.327	0.299
Be	2.07	4.02	2.09	n.a.	2.90	1.44	2.42	3.46	2.17	2.59	2.28	1.87	2.38	3.60	3.54	2.90	3.27	3.17
Cu	26.4	10.5	17.6	n.a.	16.0	29.6	29.2	12.8	10.4	44.8	12.5	12.8	34.0	8.6	21.7	18.5	6.0	15.0
Zn	69.5	65.0	n.a.	89.8	60.7	65.5	63.7	84.0	9.9	165.8	n.a.	78.0	78.2	71.8	71.5	80.2	64.6	63.8
Ga	58.6	41.7	48.5	22.0	35.4	29.3	33.7	29.8	45.6	41.8	56.3	44.4	35.5	57.0	46.3	43.6	42.7	36.6
Feeder zone mafic dike																		
	5JM2*	5JM3*	4JM10-1*	8JL406	8JL407	8JL418	Laccolith mafic dike											
							4JM24*	4JM25-1*	5JM44*	5JM46*	5JM60*	5JM64*	5JM84*	7JL152	7JL155			
<i>Major elements (wt %)</i>																		
SiO ₂	52.57	51.57	52.66	48.84	47.19	53.47	53.60	52.24	52.21	54.07	55.64	49.54	52.74	56.92	50.27			
TiO ₂	1.52	1.68	1.62	1.65	1.29	1.41	2.02	1.99	1.36	1.58	1.04	1.27	1.67	1.12	2.24			
Al ₂ O ₃	16.23	16.11	15.50	15.38	12.94	15.88	16.09	17.15	15.68	15.88	16.01	14.72	16.17	16.55	16.98			

(continued)

Table 1: Continued

	Feeder zone mafic dike						Laccolith mafic dike								
	5JM2*	5JM3*	4JM10-1*	8JL406	8JL407	8JL418	4JM24*	4JM25-1*	5JM44*	5JM46*	5JM60*	5JM64*	5JM84*	7JL152	7JL155
Fe ₂ O ₃	9.56	10.30	9.77	10.26	11.99	9.76	8.95	9.37	9.52	9.89	7.56	10.64	9.01	7.70	10.46
MnO	0.19	0.15	0.22	0.16	0.15	0.19	0.27	0.22	0.16	0.17	0.14	0.25	0.14	0.12	0.15
MgO	4.98	5.83	4.37	7.50	13.97	5.13	4.16	3.63	6.21	4.45	3.60	9.28	3.92	4.22	4.85
CaO	7.73	8.41	7.35	8.59	7.05	7.80	7.45	6.70	7.80	7.57	5.50	7.75	7.19	7.45	6.61
Na ₂ O	3.74	3.17	3.68	3.58	1.65	3.65	4.04	4.49	3.44	3.68	4.49	2.71	3.80	3.30	4.85
K ₂ O	1.77	1.39	1.68	0.57	1.00	1.25	2.26	2.36	1.41	1.65	1.80	1.61	2.03	1.78	1.80
P ₂ O ₅	0.37	0.32	0.33	0.39	0.32	0.28	0.49	0.63	0.23	0.28	0.27	0.26	0.40	0.33	0.74
LOI	1.06	0.67	1.90	2.65	2.36	1.26	0.62	0.56	1.33	0.60	3.19	1.31	2.32	0.33	0.43
Total	99.70	99.60	99.10	99.63	100.03	100.10	99.96	99.34	99.35	99.83	99.24	99.42	99.38	99.81	99.39
Mg#	50.78	52.86	46.98	59.17	69.78	51.04	47.90	43.39	56.36	47.15	48.54	63.35	46.28	52.02	47.86
<i>Trace elements (µg g⁻¹)</i>															
Ni	12.8	38.5	27.6	121.1	349.9	25.6	28.8	6.5	54.6	11.9	8.6	161.5	24.2	12.5	55.2
V	195	205	235	207	177	190	196	205	189	153	146	174	196	147	149
Cr	128	234	153	299	625	161	123	49	327	128	64	503	190	72	142
Co	48.9	56.2	53.2	41.3	71.2	26.1	46.8	49.3	63.3	35.0	31.7	68.5	45.5	23.9	29.7
Sc	26.5	27.2	26.2	26.1	23.1	30.0	21.6	17.7	25.9	20.9	20.1	23.8	22.2	21.0	15.1
Cs	3.03	1.28	4.54	0.40	1.16	1.49	4.54	10.26	4.18	2.87	6.52	11.33	2.41	2.02	1.23
Rb	64.6	38.1	63.1	11.0	23.3	35.2	76.8	96.0	46.6	36.2	128.9	71.8	60.3	51.3	35.6
Ba	330	409	337	249	209	268	453	617	252	267	249	240	417	378	428
Th	6.55	5.35	6.40	2.97	2.71	4.65	7.15	8.23	4.43	4.61	8.94	3.79	7.70	7.88	6.32
U	1.76	1.05	1.53	0.77	0.80	1.24	2.60	2.41	1.24	1.27	2.35	2.10	1.80	2.10	2.54
Nb	22.8	19.3	16.9	16.1	13.7	14.1	28.2	51.3	13.0	12.0	12.0	12.7	27.6	10.9	35.7
Ta	2.22	1.79	1.49	0.84	0.76	0.82	2.27	3.25	1.53	1.26	1.20	1.12	2.38	0.72	2.10
La	30.1	27.5	28.6	21.4	17.9	21.4	36.0	32.1	21.7	21.2	49.3	22.2	33.9	35.8	39.0
Ce	56.0	51.5	58.4	43.7	37.0	42.9	71.4	70.8	43.9	41.4	96.0	42.1	66.4	78.6	78.2
Pb	21.27	6.00	8.26	11.15	4.17	7.86	32.78	16.18	10.19	17.14	20.47	25.88	22.11	8.13	6.90
Pr	6.45	6.27	6.56	5.13	4.29	5.12	8.01	8.34	5.31	4.75	10.27	4.86	7.64	9.23	8.69
Sr	627	517	459	550	414	379	641	728	423	336	671	423	542	964	875
Nd	27.3	26.3	27.3	22.2	18.4	21.4	32.7	34.9	21.4	18.9	38.3	18.7	28.2	36.1	33.6
Hf	4.16	4.54	4.02	2.77	2.39	3.27	4.80	5.19	2.91	2.75	4.76	2.94	4.62	4.23	4.82
Zr	178	165	161	115	97	136	201	221	125	117	178	113	183	169	214
Sm	5.54	5.81	5.38	4.70	3.98	4.80	6.58	6.77	4.16	4.62	6.90	4.53	5.56	6.28	6.77
Eu	1.85	1.61	1.74	1.53	1.26	1.40	1.76	1.95	1.16	1.05	1.88	1.49	1.68	1.56	2.13
Gd	5.56	5.11	5.55	4.56	3.75	4.52	6.07	6.02	4.34	3.40	4.98	4.14	5.63	5.03	5.40
Tb	0.752	0.784	0.785	0.645	0.519	0.688	0.808	0.933	0.629	0.507	0.718	0.582	0.747	0.711	0.797
Y	25.1	25.8	26.2	20.5	16.9	23.7	25.5	27.8	20.8	18.2	22.7	20.3	24.5	21.9	24.3
Dy	4.97	4.98	4.77	4.09	3.26	4.65	5.11	5.75	4.13	3.19	4.39	3.87	4.60	3.93	4.90
Ho	0.852	0.862	0.953	0.703	0.675	0.885	0.919	0.989	0.809	0.683	0.838	0.741	0.872	0.795	0.896
Er	2.47	2.56	2.53	2.08	1.76	2.51	2.56	2.82	1.93	1.65	2.27	2.11	2.48	2.13	2.33
Tm	0.390	0.435	0.414	0.310	0.234	0.349	0.331	0.381	0.287	0.251	0.301	0.315	0.398	0.297	0.325
Yb	2.53	2.82	2.34	1.84	1.49	2.32	2.13	2.53	1.88	1.89	2.06	1.86	2.32	2.15	2.29
Lu	0.300	0.265	0.383	0.285	0.220	0.368	0.317	0.342	0.311	0.251	0.324	0.261	0.416	0.295	0.301
Be	n.a.	n.a.	1.99	1.74	1.68	1.90	2.71	1.99	n.a.	n.a.	2.78	4.14	n.a.	2.45	3.46
Cu	n.a.	n.a.	10.6	26.4	70.4	6.8	11.4	12.4	n.a.	n.a.	5.8	21.4	n.a.	13.6	27.7
Zn	121.0	86.8	110.8	154.2	121.7	113.1	151.2	130.3	91.5	74.6	93.7	145.9	134.9	309.5	n.a.
Ga	21.0	22.0	43.3	28.0	26.0	30.2	53.7	66.6	20.0	22.0	37.0	35.1	22.0	41.8	47.7

Bulk-rock analyses were acquired on glass beads by XRF and LA-ICP-MS. All samples labelled 'JM' were collected by J. Tuckermann. All others were crushed in an agate mill and analysed in the present study. n.a., not analysed; LOI, loss on ignition.

*Samples that were crushed in a tungsten carbide mill and analysed by J. Tuckermann.

Table 2: Torres del Paine mafic and felsic bulk-rock $Sr-Nd-Pb$ isotope compositions

	$^{143}Nd/^{144}Nd_i$	Nd ($\mu g\ g^{-1}$)	Sr ($\mu g\ g^{-1}$)	1SE Nd	$^{87}Sr/^{86}Sr_i$	1SE Sr	$^{206}Pb/^{204}Pb_i$	1SE $^{206}Pb/^{204}Pb$	$^{207}Pb/^{204}Pb_i$	1SE $^{207}Pb/^{204}Pb$	$^{208}Pb/^{204}Pb_i$	1SE $^{208}Pb/^{204}Pb$	aNd _i
<i>Feeder zone layered gabbro</i>													
08JL415	0.512562	14.2	454	0.000006	0.705176	0.000009	18.734	0.000	15.619	0.000	38.630	0.001	-1.17
08JL435	0.512616	7.8	747	0.000011	0.704913	0.000025	18.708	0.001	15.621	0.001	38.618	0.002	-0.12
<i>Feeder zone Px-Hbl gabbro</i>													
05JM4	0.512715	12.9	496	0.000005	0.704843	0.000003	18.653	0.002	15.575	0.001	38.447	0.004	1.82
05JM9*	0.512689	15.3	714	0.000004	0.704502	0.000020	18.686	0.001	15.615	0.001	38.579	0.001	1.30
<i>Laccolith lower Hbl-gabbro</i>													
07JL149	0.512754	21.8	413	0.000008	0.704098	0.000027	18.705	0.001	15.615	0.001	38.591	0.002	2.58
07JL154	0.512765	33.9	782	0.000005	0.703913	0.000003	18.705	0.016	15.650	0.013	38.688	0.033	2.80
07JL156	0.512765	31.6	797	0.000003	0.704043	0.000004	n.a.	n.a.	n.a.	n.a.	n.a.	n.a.	2.78
<i>Laccolith upper Hbl-gabbro</i>													
05JM29	0.512745	19.3	499	0.000001	0.704155	0.000005	18.700	0.003	15.652	0.002	38.701	0.006	2.40
07JL158	0.512760	25.2	637	0.000720	0.704086	0.000008	n.a.	n.a.	n.a.	n.a.	n.a.	n.a.	2.68
07JL160	0.512712	21.9	570	0.000007	0.704257	0.000006	18.659	0.000	15.579	0.000	38.472	0.001	1.76
<i>Feeder zone diorite</i>													
08JL419	0.512699	28.1	655	0.000004	0.704409	0.000008	18.711	0.000	15.640	0.000	38.667	0.001	1.50
<i>Laccolith diorite</i>													
05JM33	0.512759	38.0	778	0.000006	0.704000	0.000006	18.683	0.001	15.593	0.001	38.524	0.003	2.67
07JL36	0.512785	36.3	1015	0.000001	0.703941	0.000005	18.703	0.003	15.654	0.002	38.702	0.005	3.18
07JL151	0.512676	34.3	572	0.000004	0.704374	0.000012	18.746	0.017	15.667	0.015	38.770	0.037	1.06
08JL390	0.512676	27.4	495	0.000008	0.704125	0.000137	18.739	0.001	15.631	0.001	38.653	0.001	1.06
<i>Feeder zone mafic dike</i>													
08JL407	0.512734	18.4	414	0.000004	0.704274	0.000034	18.719	0.001	15.625	0.001	38.622	0.001	2.19
<i>Laccolith mafic dike</i>													
07JL155	0.512761	33.6	875	0.000003	0.703880	0.000003	18.648	0.001	15.620	0.000	38.590	0.001	2.71
<i>Unit I granite</i>													
05JM68	0.512667	23.9	85	0.000007	0.705179	0.000004	n.a.	n.a.	n.a.	n.a.	n.a.	n.a.	0.88
05JM80	0.512665	42.3	70	0.000004	0.704630	0.000006	18.690	0.000	15.583	0.000	38.496	0.000	0.84
<i>Unit II granite</i>													
04JM22	0.512581	34.4	187	0.000009	0.705322	0.000017	n.a.	n.a.	n.a.	n.a.	n.a.	n.a.	-0.80
04JM31	0.512601	35.8	162	0.000007	n.a.	n.a.	18.769	0.001	15.648	0.001	38.740	0.002	-0.42
<i>Unit III granite</i>													
05JM8	0.512601	28.8	201	0.000002	0.705123	0.000002	n.a.	n.a.	n.a.	n.a.	n.a.	n.a.	-0.40
05JM62	0.512635	28.3	194	0.000022	0.705172	0.000008	18.719	0.000	15.598	0.000	38.550	0.001	0.26
07JL173	0.512628	29.9	305	0.000013	0.704866	0.000003	18.713	0.000	15.587	0.000	38.518	0.001	0.11
<i>Porphyric granite</i>													
07JL102	0.512630	30.2	520	0.000172	0.704725	0.000006	18.707	0.000	15.591	0.000	38.529	0.001	0.15
07JL104	0.512641	23.6	353	0.000008	0.704782	0.000005	18.740	0.005	15.643	0.004	38.670	0.011	0.38
07JL122	0.512580	32.1	269	0.000006	0.704586	0.000004	18.692	0.000	15.591	0.000	38.542	0.000	-0.82

Radiogenic ratios acquired on bulk rock powders. JM samples were collected by J. Tuckermann and analysed by J. Leuthold.

*Samples crushed in a tungsten carbide mill and analysed by J. Tuckermann.

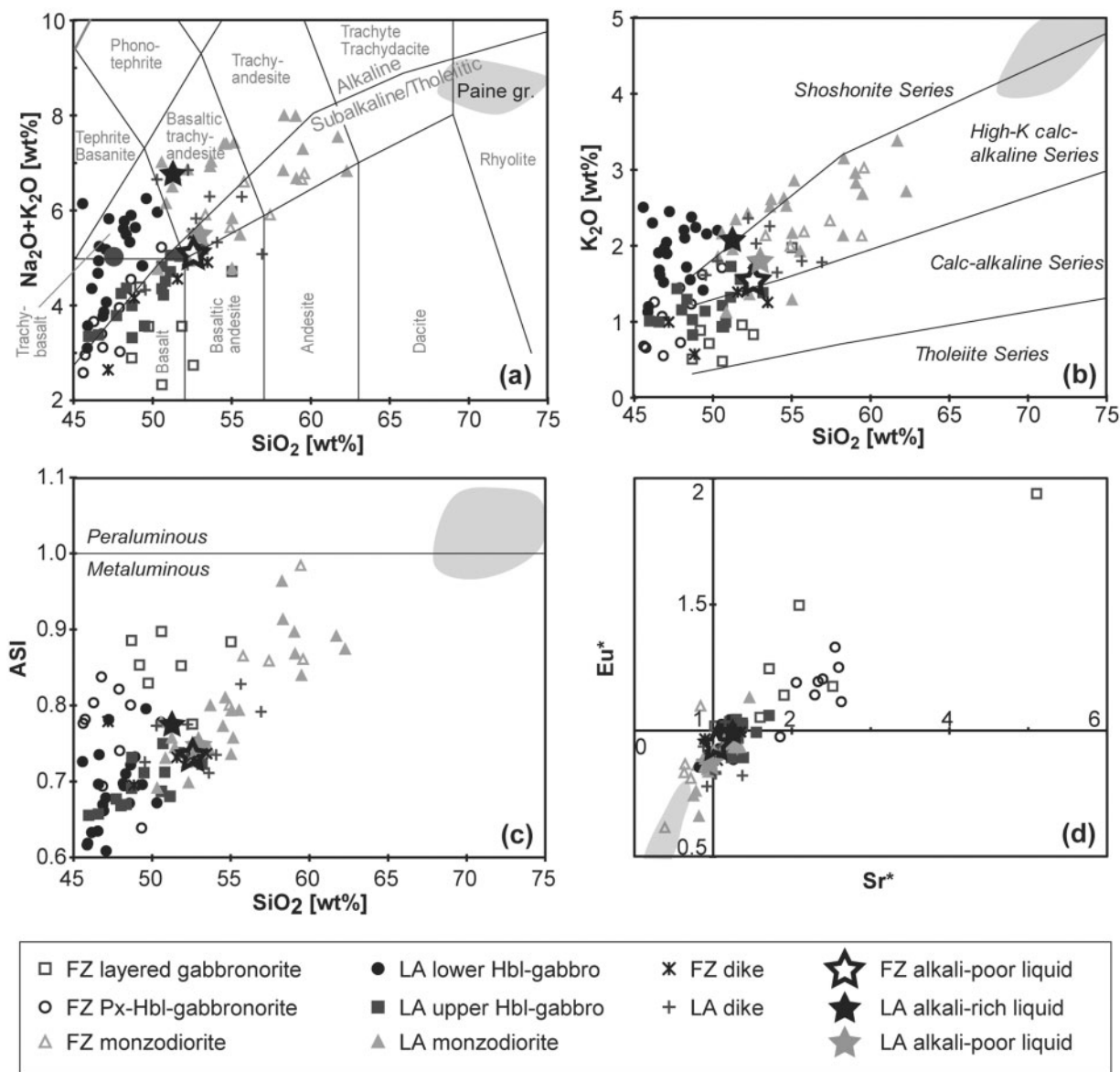


Fig. 5. The mafic rocks (PMC) of the TPIC can be clearly grouped and separated into different trends for the feeder zone and the mafic laccolith using (a) TAS (Le Bas *et al.*, 1986) and (b) K_2O vs SiO_2 diagrams: the FZ layered gabbronorites are calc-alkaline, whereas the FZ pyroxene–hornblende-gabbronorite, the LA upper hornblende-gabbro and LA ‘alkali-poor’ monzodiorite are high-K calc-alkaline, and the LA lower hornblende-gabbro and LA ‘alkali-rich’ monzodiorites follow a high-K calc-alkaline to shoshonitic trend. (c) PMC samples are metaluminous whereas granite samples are peraluminous in an ASI $[Al/(Ca + Na + K)]$ vs SiO_2 diagram. (d) Strongly positive Sr and Eu anomalies are observed in the feeder zone layered gabbronorite and pyroxene–hornblende gabbronorite, whereas the feeder zone monzodiorite and granites display negative Sr and Eu anomalies. $Sr^* = Sr_n/[1/2(Pr_n + Nd_n)]$ and $Eu^* = Eu_n/[1/2(Sm_n + Gd_n)]$ where subscript n indicates normalized to CI chondrite. The grey areas are TPIC granitic rocks from Michael (1984), Michel *et al.* (2006) and Baumgartner *et al.* (2007).

and Michael, 1984, 1991; Michel *et al.*, 2006). All samples are characterized by distinct positive Pb anomalies, weak negative Nb and Ta values, and chondrite-normalized La/Yb values >6 . La/Nb and Ba/Th ratios are intermediate between typical mid-ocean ridge basalt (MORB) and calc-alkaline suites, with similar average values for all PMC units of ~ 13 and ~ 75 , respectively.

Feeder zone (FZ) gabbronorites

The layered gabbronorites show significant chemical variations. They display an initial strong CaO and Al_2O_3 decrease over only ~ 5 wt % SiO_2 . This is related to modal variations in Ca-rich plagioclase, orthopyroxene and clinopyroxene. This is supported by well-developed, positive Sr and Eu anomalies (Fig. 5d, and see also Fig. 8), suggesting plagioclase accumulation. The large variability of Sc at a

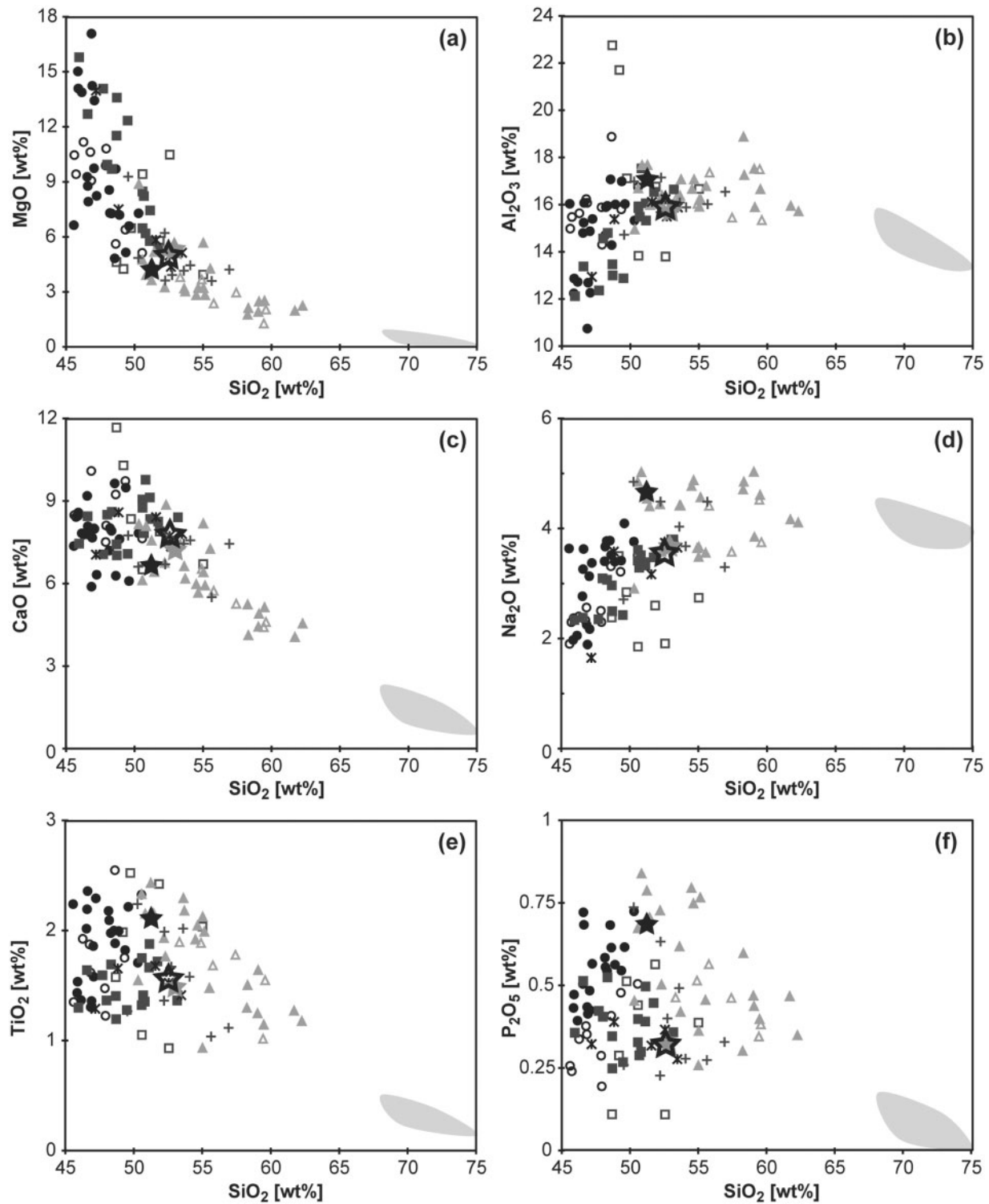


Fig. 6. Selected binary major element vs SiO_2 plots (in wt %) for the Torres del Paine mafic rocks. Grey fields correspond to the Paine granite of Michael (1984), Michel *et al.* (2006) and Baumgartner *et al.* (2007). Symbols as in Fig. 5.

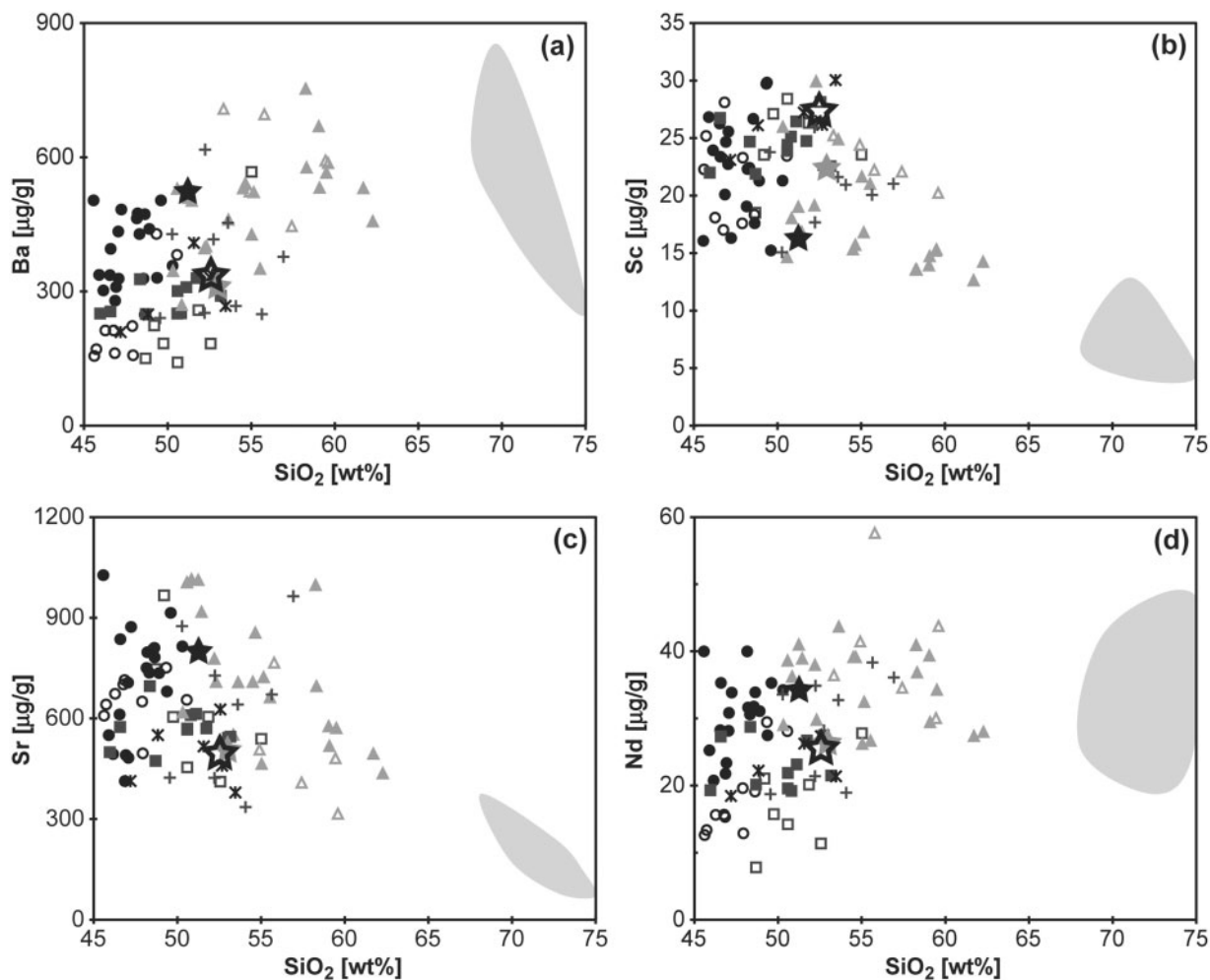


Fig. 7. Selected trace element variations ($\mu\text{g g}^{-1}$) vs SiO_2 (wt %) diagrams for the Torres del Paine mafic rocks. (a) Ba vs SiO_2 . (b) Sc vs SiO_2 (note that monzodiorites display a negative correlation for $\text{SiO}_2 > 53$ wt %, indicating fractionation of Fe–Mg minerals). (c) Sr vs SiO_2 ; Sr generally decreases for rocks with more than 55 wt % SiO_2 , indicating that the Si-rich monzodiorites have fractionated some plagioclase. (d) Nd vs SiO_2 ; Nd remains roughly constant with increasing SiO_2 . Grey fields correspond to the Paine granite of Michael (1984), Michel *et al.* (2006) and Baumgartner *et al.* (2007). Symbols as in Fig. 5.

given SiO_2 concentration is controlled by the modal amount of clinopyroxene (Fig. 7b). The layered gabbronorites are at the lower end of the range of Na_2O , K_2O and P_2O_5 concentration of the other mafic rocks, and display the lowest total alkali contents of the TPIC in the total alkalis–silica (TAS) diagram (Fig. 5a). The MgO contents (Fig. 6a) of the FZ gabbronorites are lower than those of the laccolith hornblende-gabbros. They are also Ba-poor (Fig. 7a) and have lower abundances of other incompatible trace elements. In contrast, their Aluminium Saturation Index [ASI, $\text{Al}_2\text{O}_3/(\text{CaO} + \text{Na}_2\text{O} + \text{K}_2\text{O})$], Sr^* and Eu^* [$\text{Sr}^* = \text{Sr}_n/[(\text{Pr}_n + \text{Nd}_n)]$ and $\text{Eu}^* = \text{Eu}_n/[(\text{Sm}_n + \text{Gd}_n)]$] ratios are higher (Fig. 5c and d).

The FZ pyroxene–hornblende gabbronorites are very similar in composition to the FZ layered gabbronorites, but they have lower SiO_2 and slightly higher MgO . FZ

pyroxene–hornblende gabbronorites also display positive Sr and Eu anomalies and a large Sc variability (Figs 5d and 7b), indicating plagioclase and pyroxene modal variations.

Laccolith (LA) hornblende-gabbros

The LA lower hornblende-gabbros are high-K calc-alkaline to shoshonitic in composition and have the highest K_2O contents of all PMC rocks, with K/Na ratios between 0.46 and 1.25. They have the highest TiO_2 , Na_2O , K_2O , P_2O_5 and Ba contents when compared with the other laccolith gabbros (Figs 6 and 7a). This can be explained by higher modal amounts of biotite and apatite. Their $\text{Mg}\#$ is distinctly higher than that of the FZ gabbronorites; Sr contents are highly variable, but correlate with Al_2O_3 . The Sc contents decrease from the most mafic

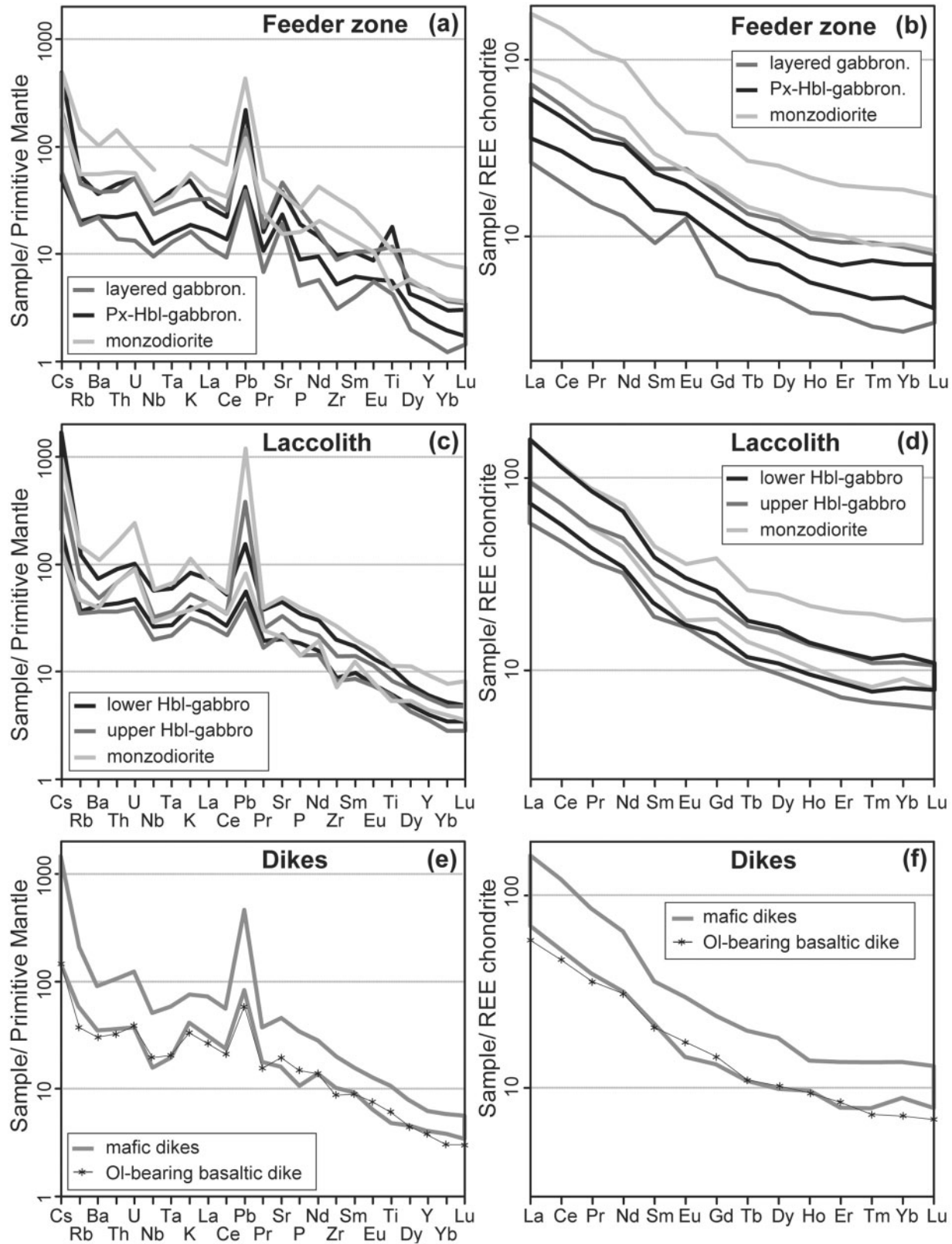


Fig. 8. Primitive mantle-normalized trace element patterns and chondrite-normalized REE patterns for feeder zone gabbros and associated monzodiorites (a, b), laccolith gabbros and associated monzodiorites (c, d) and dikes (e, f).

to the most felsic hornblende-gabbro samples (Fig. 7b). The lower hornblende-gabbros have high trace element concentrations, as seen in primitive mantle and chondrite-normalized diagrams (Fig. 8), with pronounced negative Nb and Ta anomalies.

The upper hornblende-gabbros of the laccolith belongs to the calc-alkaline to high-K calc-alkaline series, with K/Na ratios ranging between 0.24 and 0.68. These rocks display a more modest increase in Al_2O_3 , Sr and Ba with increasing SiO_2 , relative to the lower hornblende-gabbros. This mainly reflects early plagioclase fractionation and the scarcity of biotite in these gabbros (Figs 6 and 7). The Sc contents are relatively constant and similar to the highest concentrations in the lower hornblende-gabbros. The trace element enrichment of the upper hornblende-gabbros is similar to that of the most evolved FZ pyroxene-hornblende gabbro. Nb and Ta display a distinct negative anomaly (Fig. 8).

Monzodiorites (feeder zone and laccolith)

The chemical differences described above between the FZ pyroxene-hornblende gabbro, LA lower hornblende-gabbro and LA upper hornblende-gabbro are also reflected in the associated dioritic rocks. All monzodiorites from the feeder zone are relatively low in K_2O , Na_2O , TiO_2 , P_2O_5 and Sr but higher in Sc (Figs 6 and 7). They display the highest Fe/Mg ratios of the monzodiorites of the PMC. Except for Cs, Pb and Sr, the FZ monzodiorites display 2–3 times higher trace element concentrations relative to the FZ pyroxene-hornblende gabbro and layered gabbro (Fig. 8). Such chemical differences between the monzodiorites and hornblende-gabbros are not obvious in the laccolith PMC. The monzodiorites in the laccolith span a large range in alkali contents that correlate with TiO_2 , P_2O_5 and Sr. The alkali-rich rocks of the LA have trace element concentration similar to FZ monzodiorites. Subtle negative Nb, Ta, Ba, and Ti anomalies are observed in FZ and LA monzodiorites. The feeder zone and uppermost monzodiorites display on average the highest REE concentrations. However, the monzodiorites do not show systematic chemical variations from the bottom to the top of the mafic complex and different compositions can be found next to each other. Weak negative Eu anomalies are observed in some monzodiorites and Sr anomalies may be positive or negative (Fig. 5d).

Granites (feeder zone and laccolith)

Bulk-rock compositions of the Paine granites have been reported by Michael (1984), Michel *et al.* (2006) and Baumgartner *et al.* (2007). A distinct compositional gap exists between the mafic rocks and the granites between 62 and 68 wt % SiO_2 (Figs 5–7). Their bulk-rock compositions show the same trends as the PMC samples. On chondrite-normalized REE diagrams, the typical Paine granite units are not more than four times more enriched than the most primitive mafic rocks, with the exception of

Eu (Fig. 8). Ba and Sr decrease with increasing SiO_2 (Fig. 7a and c). All the granites display large negative Sr and Eu anomalies (Fig. 5d).

Dikes (feeder zone and laccolith)

The mafic dikes are basaltic (trachy-)andesites with between 49 and 56 wt % SiO_2 . They plot between the hornblende-gabbros and monzodiorites on most diagrams, showing significant overlap with the low- SiO_2 monzodiorites (Figs 5–7). The dikes generally follow the same chemical trends as the associated plutonic rocks. Only one olivine-bearing dike (08JL407) has a basaltic composition. It is similar to the most mafic samples of the Torres del Paine complex, with 47 wt % SiO_2 , 14 wt % MgO (molar Mg# = 70), $350 \mu\text{g g}^{-1}$ Ni and $625 \mu\text{g g}^{-1}$ Cr. Despite its bulk-rock basaltic composition, its fine-grained groundmass has a basaltic andesite composition, similar to many other dikes. This sample is clearly more mafic than all the other TPIC dikes. It is necessary to explore whether it corresponds to the TPIC most primitive liquid or if its composition has resulted from olivine accumulation. Using Fe-Mg and Ni partition coefficients between olivine and liquid, determined by Ulmer (1989) and Kinzler *et al.* (1990), it appears that this dike contains accumulated olivine and cannot be used as a TPIC primary liquid (Leuthold *et al.*, in preparation).

SUMMARY

The gabbroites and monzodiorites from the feeder zone display on average a larger variation in REE and other incompatible trace elements when compared with rocks from the laccolith. The shape and enrichment of the pyroxene-hornblende gabbroite trace element patterns are broadly similar to those of the layered gabbroites. The positive Sr and Eu anomalies in the FZ gabbros relative to the laccolith can be attributed to plagioclase accumulation, which is expressed by large modal variations ranging from leucocratic anorthosite to pyroxene-hornblende gabbroite. The positive Eu anomaly is highest in plagioclase-rich rocks and decreases progressively with increasing pyroxene content. Clinopyroxene accumulation is reflected by high Ca and Sc contents.

The lower hornblende-gabbros and upper hornblende-gabbros in the laccolith can be distinguished on the basis of different K_2O , Na_2O , P_2O_5 and Ba contents. These elements are enriched in the lower hornblende-gabbros owing to higher modal biotite and apatite contents. In the lower hornblende-gabbros, the late appearance of plagioclase, after hornblende, induces an Al_2O_3 and Sr increase at low SiO_2 . Nb and Ta negative anomalies are more pronounced in the LA lower and upper hornblende-gabbros, relative to the FZ pyroxene-hornblende gabbroites and layered gabbroites. Monzodiorite samples extend the chemical trends defined by the FZ pyroxene-hornblende

gabbronorites, LA lower hornblende-gabbros and LA upper hornblende-gabbros.

BULK-ROCK ISOTOPIC COMPOSITION

The Sr, Nd and Pb isotopic compositions of the TPIC rocks (Table 2, Fig. 9) show correlated variations in Nd–Sr (initial $^{87}\text{Sr}/^{86}\text{Sr}_i = 0.70388\text{--}0.70532$; $^{143}\text{Nd}/^{144}\text{Nd}_i = 0.512562\text{--}0.512785$) but smaller variations in $^{206}\text{Pb}/^{204}\text{Pb}_i$ (18.65–18.77) and $^{207}\text{Pb}/^{204}\text{Pb}_i$ (15.58–15.67). The PMC and granitic samples plot along a continuous trend, from the most primitive laccolith samples to the more evolved feeder zone and granitic rocks (Fig. 9a). The Torres del Paine granites have slightly higher $^{206}\text{Pb}/^{204}\text{Pb}_i$ than most of the TPIC mafic rocks (Fig. 9). Overall, the data show a weak enrichment relative to the basalts from the Chile Ridge (e.g. Karsten *et al.*, 1996), trending towards the EMII reservoir and/or the Patagonian continental crust, with possibly some component of the EM1 reservoir. The LA lower hornblende-gabbros and LA alkali-rich monzodiorites seem to have more depleted Sr and Nd isotopic compositions compared with LA upper hornblende-gabbros and LA alkali-poor monzodiorites. The FZ layered gabbronorites have the most radiogenic Sr isotope compositions of the mafic rocks. Unit I granite seems to be the least radiogenic, whereas a single Unit II sample shows the highest $^{87}\text{Sr}/^{86}\text{Sr}_i$ value.

DISCUSSION

Relationship among the TPIC units

The characteristic features of the laccolith PMC are its undulating contacts as well as the presence of schlieren, and diffuse rather than sharp contacts between gabbros and monzodiorites. The distinction between different mafic units is complicated by their similar trace element chemistry. Nearly complete vertical sections through the mafic complex in the laccolith allowed us to distinguish between lower and upper hornblende-gabbros, associated with alkali-rich and alkali-poor monzodiorites. The occurrence of centimetre-scale granodioritic diapirs ascending from dioritic sills into the partially crystallized, overlying gabbroic unit indicates that high temperatures prevailed over sufficient time intervals to preserve ‘ductile’ contacts. Layered gabbronorite, pyroxene–hornblende gabbronorite and alkali-poor monzodiorite are found in the feeder zone (Fig. 2). An important issue is how the subvertical units in the feeder zone can be related to those of the laccolith.

In the following sections, we discuss the origin of the primitive TPIC liquids, the links between the mafic rocks and associated granites, as well as the connection between the feeder zone and the laccolith.

High-K calc-alkaline and shoshonitic series Feeder zone

The layered gabbronorite and pyroxene–hornblende gabbronorite have comparable incompatible element ratios, similar REE patterns and distinct cumulate signatures owing to plagioclase and pyroxene accumulation (Figs 5d and 8). Field observations demonstrate syn-intrusive contacts between the two gabbros, and dated zircon grains from pegmatoid pods have similar ages within their uncertainties (Leuthold *et al.*, 2012). We thus propose that they are co-magmatic. In addition to their textures, the main difference between the two gabbros is in the modal proportion of pyroxene and hornblende: hornblende forms up to 40% of the pyroxene–hornblende gabbronorites, whereas it is a late interstitial phase not exceeding 20% in the layered gabbronorites. The distinction between the units is not always obvious, as all kinds of intermediate variations exist between the two end-members. The modal amount of hornblende is due to the progressive replacement of olivine and clinopyroxene and/or orthopyroxene by hornblende, according to the peritectic reactions $\text{Cpx} + \text{Liq} = \text{Hbl}$, $\text{Opx} + \text{Liq} = \text{Hbl}$, or $\text{Ol} + \text{Liq} = \text{Hbl}$, which mainly depend on the liquid Na_2O and H_2O content (Sisson & Grove, 1993). This indicates that the layered gabbronorites crystallized from a melt that was relatively dry compared with the pyroxene–hornblende gabbronorites. The positive Eu anomaly gradually decreases with progressive REE enrichment in the FZ layered gabbronorites and FZ pyroxene–hornblende gabbronorites. This indicates various amounts of trapped intercumulus liquid. We therefore interpret the two FZ gabbros to be cumulates with variable trapped melt fractions.

Laccolith

An alkali-rich (shoshonitic) suite can be distinguished in a K_2O versus SiO_2 diagram (Fig. 5b). The lower hornblende-gabbros and alkali-rich monzodiorites show a characteristic enrichment in Na_2O , K_2O , TiO_2 , P_2O_5 and Sr, low Sc contents, and similar incompatible trace element ratios (Figs 5–7). Thin-section observations show that this is largely reflected in a higher percentage of modal biotite and apatite compared with the other hornblende-gabbros and monzodiorites. The fine-grained, interstitial mineral assemblage of the hornblende-gabbros has the same mineralogy as the alkali-rich monzodiorites. The limited chemical variability between the lower hornblende-gabbros and monzodiorites, as well as the similarities between their groundmass mineralogy, indicates incomplete extraction of interstitial liquid from the hornblende-gabbro sills. Similar observations have been made for the LA upper hornblende-gabbros and the alkali, TiO_2 , P_2O_5 and Sr-poor monzodiorites. Incomplete extraction of interstitial liquid explains the limited chemical variability between the hornblende-gabbros and monzodiorites.

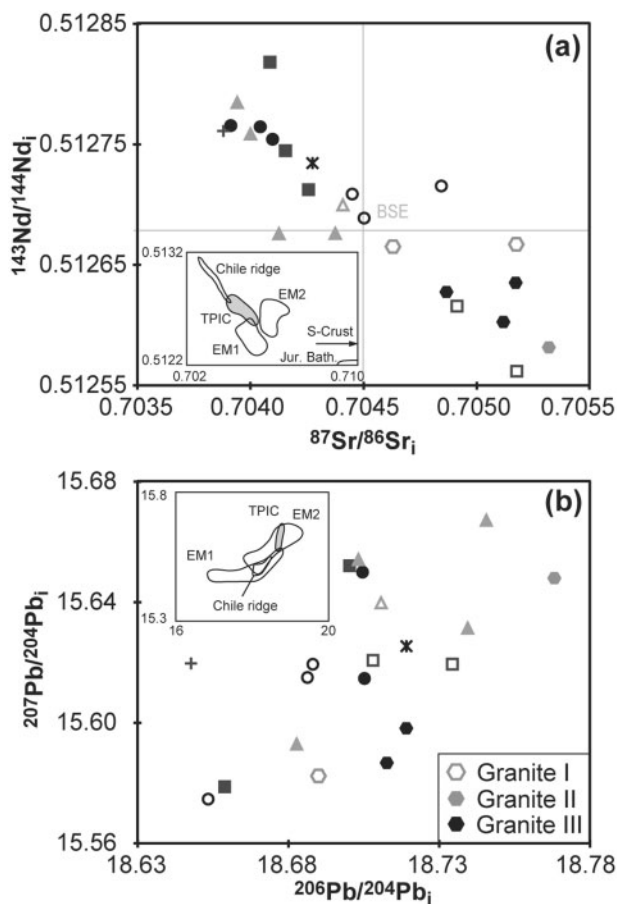


Fig. 9. (a) Variation of $^{143}\text{Nd}/^{144}\text{Nd}$ vs $^{87}\text{Sr}/^{86}\text{Sr}$ for bulk Paine plutonic rock: variations between the different rock types of the TPIC are very small. Inset shows Chile ridge MORB (Karsten *et al.*, 1996), Patagonian Batholith (Hervé *et al.*, 2007), EM1, EM2 mantle end-members (Hofmann, 1997) and Patagonian S-type crust (Kilian & Behrmann, 2003) for comparison with the TPIC rocks. (b) $^{207}\text{Pb}/^{204}\text{Pb}$ vs $^{206}\text{Pb}/^{204}\text{Pb}$ for the Paine rocks. Inset shows Chile ridge MORB (Karsten *et al.*, 1996) and EM1 and EM2 (Hofmann, 1997) mantle end-members for comparison with the TPIC rocks. Symbols as in Fig. 5.

Mingled contacts and the observed geochemical similarities suggest a cogenetic origin for the hornblende-gabbros and monzodiorites. It has to be pointed out that monzodiorites of a given composition are not spatially related to a specific gabbroic unit and may occur as single sills, and they form the uppermost unit of the Paine mafic sill complex (see Fig. 2).

Parental magma geochemistry

The composition of the post-plutonic dikes might provide a reasonable estimate of the parental magma composition (e.g. Upton *et al.*, 2002). Michael (1991) previously proposed that some dikes may be considered as near-parental liquids. Most dikes contain neither enclaves nor resorbed crystals, indicating the absence of magma mingling and

mixing. They have a fine-grained groundmass suggesting fast cooling and thus minimal *in situ* fractionation. The observed chemical variation between the mafic dikes (i.e. different alkali or SiO_2 contents; see Figs 5–7) raises the question of potential source heterogeneities. The variation in the alkali and H_2O content of the source is probably responsible for the observed differences between the shoshonitic and high-K calc-alkaline series of the TPIC mafic complex and its distinct fractionation sequences. Here we assume that only insignificant amounts of interstitial liquid escaped from the dikes and that no mixing and mingling occurred. We then calculate averages for the shoshonitic dikes, and feeder zone and laccolith high-K mafic dikes. Estimated liquid compositions are basaltic trachyandesite and high-K basaltic trachyandesite. Only subtle differences (e.g. Sc, see Fig. 7b) are found between the laccolith and the feeder zone alkali-poor dikes. The estimated liquid compositions are suitable parental magma compositions from which the TPIC mafic rocks could have crystallized. We present below AFC and FC models to test if the TPIC intermediate and felsic magmas could be derived from basaltic trachy-andesitic parental magmas.

Parental magma isotopic composition

The isotopic compositions of the most primitive TPIC mafic rocks suggest that the primitive magmas were derived from a slightly enriched mantle source. Alternatively, they could have been derived from normal depleted mantle and modified by crustal assimilation. The presence of an enriched mantle source in Patagonia is well documented by isotopic data for the younger main-plateau and post-plateau lavas and mantle xenoliths from the Pali Aike volcanic field (D'Orazio *et al.*, 2000; Gorrington & Kay, 2001).

The layered gabbronorite unit displays the highest $^{87}\text{Sr}/^{86}\text{Sr}_i$ and lowest $^{143}\text{Nd}/^{144}\text{Nd}_i$ composition. This is consistent with field observations that revealed the presence of small, partially molten crustal xenoliths in the FZ layered gabbronorite (Fig. 3b). Granites and FZ pyroxene–hornblende gabbronorites also display moderately radiogenic $^{87}\text{Sr}/^{86}\text{Sr}_i$ values. In the latter, there is no field evidence for enclaves of crustal xenoliths or xenocrysts, but anhedral reversely zoned plagioclase cores have been documented. Putlitz *et al.* (2006) have reported high $\delta^{18}\text{O}$ values for primary phases such as olivine (5.9‰), pyroxene (6.7‰) and hornblende (6.4‰) in pyroxene–hornblende gabbronorite samples, which is thought to reflect the early stages of contamination by crustal material or fluids.

Possible sources of contamination are the Jurassic felsic plutons of the Jurassic Patagonian batholith [mean values of $^{87}\text{Sr}/^{86}\text{Sr} \sim 0.7085$ and $^{143}\text{Nd}/^{144}\text{Nd} \sim 0.51218$, recalculated to 12.5 Ma from Hervé *et al.* (2007), with $22.5 \mu\text{g g}^{-1}$ Nd and $191 \mu\text{g g}^{-1}$ Sr], or the Tobifera Formation, which consists of voluminous silicic volcanic rocks of similar age, geochemistry and isotope geochemistry (mean values of

$^{87}\text{Sr}/^{86}\text{Sr} \sim 0.7075$ and $^{143}\text{Nd}/^{144}\text{Nd} \sim 0.51223$; Hervé *et al.*, 2007) (Fig. 9a). Alternatively, Patagonian S-type crust (Kilian & Behrmann, 2003; estimated value of $^{87}\text{Sr}/^{86}\text{Sr}$ 0.72184, and $^{143}\text{Nd}/^{144}\text{Nd}$ 0.51232, with $28.6 \mu\text{g g}^{-1}$ Nd and $173 \mu\text{g g}^{-1}$ Sr) may have been assimilated. Paleozoic schists, exposed on the east coast of Patagonia, could be another alternative. They have heterogeneous isotopic compositions ($^{143}\text{Nd}/^{144}\text{Nd}$ 0.51228–0.51219, $^{87}\text{Sr}/^{86}\text{Sr}$ 0.7156–0.7287, Nd $14.5\text{--}38.4 \mu\text{g g}^{-1}$, Sr $167\text{--}301 \mu\text{g g}^{-1}$; Pankhurst *et al.*, 2003). PMC samples are intermediate between EMI and the Chile Ridge basalts on Pb isotope ratio diagrams (mean $^{206}\text{Pb}/^{204}\text{Pb} \sim 18.1$ and $^{207}\text{Pb}/^{204}\text{Pb} \sim 15.5$, Karsten *et al.*, 1996; Kilian & Behrmann, 2003) and EMII.

We conclude that the different parental magmas are involved in the petrogenesis of the PMC samples, resulting in subtle geochemical and isotopic differences. (1) We propose that the FZ gabbronorite cumulates crystallized from a high-K calc-alkaline basaltic trachyandesitic magma. This has experienced contamination at high temperatures, near the liquidus, as even early crystallized olivine displays some sign of contamination (Putlitz *et al.*, 2006). The FZ layered gabbronorites record additional contamination owing to partial assimilation of crustal xenoliths. (2) The mafic rocks that follow a shoshonitic differentiation trend crystallized from a parental magma that is similar to the shoshonitic 07JL155 mafic dike, which is the least radiogenic PMC sample. (3) The LA upper hornblende-gabbro crystallized from a high-K calc-alkaline basaltic trachyandesitic liquid.

Age relations between the mafic cumulates and granites

FZ pyroxene–hornblende gabbronorite zircon grains from pegmatitic pods have been dated to 12.593 ± 0.009 Ma by TIMS, and a pegmatite from the layered gabbronorite has been dated to 12.587 ± 0.009 Ma (Leuthold *et al.*, 2012). The emplacement ages of the Unit I granite of Michel *et al.* (2008) have been recalculated to yield 12.58 ± 0.02 Ma and 12.58 ± 0.01 Ma (Leuthold *et al.*, 2012). The feeder zone mafic rocks and the oldest Unit I granite have thus the same age, within uncertainties. Their average isotopic composition is similar and the geochemical signatures of the FZ gabbronorites display evidence for melt segregation. We thus propose that the FZ gabbronorites represent the complementary cumulates that crystallized during the formation of the Unit I granite.

The Paine granitic sill complex (12.58 ± 0.02 Ma for Unit I, and 12.49 ± 0.02 Ma for Unit III; Michel *et al.*, 2008; Leuthold *et al.*, 2012) is older than the underlying mafic sill complex, dated to 12.472 ± 0.009 Ma to 12.431 ± 0.006 Ma (Leuthold *et al.*, 2012). This indicates that the mafic sill complex exposed today does not correspond to a fractionated cumulate linked to the Paine granites I and II. However, we cannot exclude the possibility that Unit III granite and lower hornblende-gabbro

magmas might have coexisted, as their crystallization ages overlap within uncertainties. Below, we test these hypotheses with simple fractional crystallization (FC) and combined assimilation plus fractional crystallization (AFC) models.

FC and AFC models

Sisson *et al.* (2005) discussed the volume problem between related mafic and granitic liquids, showing that only 12–25 wt % of felsic liquid can be produced either by crystal fractionation or by partial melting of a mafic source. The exposed volumes observed in the TPIC are incompatible with such a percentage. The granitic rocks represent $\sim 80 \text{ km}^3$ and mafic rocks only $\sim 8 \text{ km}^3$, corresponding to ~ 90 vol. % granite (Leuthold *et al.*, 2012). Below, we use modelling results and recently obtained high-resolution U–Pb zircon age data (Michel *et al.*, 2008; Leuthold *et al.*, 2012) in an attempt to reconcile this apparent discrepancy.

We investigate the origins of the TPIC monzodiorites and the Unit III and Unit I granites by AFC and FC modelling using the IgPet software (Carr, 2012). We used estimated bulk-partition coefficients from the phase proportions of the fractionated assemblages (i.e. if plagioclase is fractionated, the bulk Sr partition coefficient is >1 and becomes $\gg 1$ if the cumulate is an anorthosite), wall-rock assimilation rate (dM_a , mass per unit time) and fractionation rate (dM_{fc} , mass per unit time). From a practical perspective, we assumed minimum and maximum partition coefficients for Sr and Nd. This was found to be necessary to reproduce the compositional range of all the monzodiorites, Unit I and Unit III granite. We varied the ratio of the rate of assimilation to fractionation ($r = dM_a/dM_{fc}$) from 0 to 0.25. An r ratio of 0.25 is a reasonable maximum estimate for assimilation of pelite or granite wall-rock, which has a temperature of 400°C , by a basaltic andesite magma crystallizing to dacite (i.e. from 1050 to 900°C) (Matile *et al.*, 2000). The value of r starts to decrease at lower crystallization temperatures, similar to those expected for the TPIC granite (Matile *et al.*, 2000). In addition, the AFC model solutions have to be consistent with the $^{143}\text{Nd}/^{144}\text{Nd}$, $^{87}\text{Sr}/^{86}\text{Sr}$, Nd and Sr compositions of the final products. We have also maintained a residual liquid fraction ($F > 0.2$).

Laccolith monzodiorites.

Different types of monzodiorite have been identified in the field: they are intruded as sills within the LA hornblende-gabbros, and also form a distinct unit at the top of the mafic sill complex. The occurrence of monzodiorite as injected sills within the previously emplaced upper and lower hornblende-gabbro sills shows that they do not only form by segregation from hornblende-gabbro sills within the laccolith. The overlapping compositional domains between the most primitive monzodiorites and the most evolved mafic dikes (Figs 5–7) could also be

taken as an indication that some of the monzodiorite magmas originated beneath the present-day exposure levels of the Torres del Paine mafic complex. On the other hand, the fine-grained groundmass of the LA hornblende-gabbros and the limited chemical variability between the LA hornblende-gabbros and LA monzodiorites indicate incomplete extraction of interstitial liquid from LA hornblende-gabbro sills. The field observations showing transitions from hornblende-gabbro to monzodiorite and rarely granodiorite within a single sill can be taken as an argument for interstitial liquid segregation after magma emplacement within the laccolith. FC models have been used to test if fractionation processes from the estimated parental liquids (as represented by dikes) can result in hornblende-gabbro cumulates and differentiated monzodiorites (Fig. 10a and b).

The calculations show that it is difficult to model a single fractionation trend, at least for the lower hornblende-gabbro sills (Fig. 10a). The Sr and Nd concentrations of the monzodiorites and hornblende-gabbros define the subparallel trends and modelling critically depends on the estimated parental magma composition. The large variation of Sr in the lower hornblende-gabbros is best explained by modal variations of plagioclase and highly variable trapped melt fractions. The parental liquid composition for the high-K calc-alkaline series is less Sr-rich. Modelling the monzodiorites as derivatives from fractionating upper hornblende-gabbros (Fig. 10b) indicates a moderately incompatible behaviour for Sr and Nd.

Feeder zone mafic rocks—Unit I granite.

We also present a fractional crystallization model between the FZ gabbronorites and the FZ monzodiorites (Fig. 10c) and the laccolith Unit I granite (Fig. 10d). This is based on field evidence, zircon ages and the distinct cumulate geochemical signature of the FZ mafic rocks. The mineralogical composition of leucocratic channels from the layered gabbronorite corresponds to the adjacent FZ monzodiorites. Also, the FZ pyroxene–hornblende gabbronorite isotopic composition is similar to that of the Unit I granite and the FZ monzodiorites. The moderately radiogenic Sr isotope signature of those units was discussed above and interpreted to reflect early stages of contamination by crustal material or fluids. Because of the similar isotopic compositions, there is no need to invoke additional assimilation for modelling the gabbronorite–granite I relationships. Bulk partition coefficients were estimated from the general chemical trends of the TPIC series (see Fig. 7) and results are presented in Fig. 10c and d. In contrast to the models presented above, the differentiation from a high-K basaltic trachyandesitic liquid to form monzodiorite requires Nd to be strongly incompatible. The trend between the FZ gabbronorites and monzodiorites in the Nd vs SiO₂ Harker diagram (Fig. 7d) indicates that Nd is

indeed incompatible. This is in agreement with the low hornblende content of the layered gabbronorites. Bulk Nd compatibility progressively increases for liquids saturated with hornblende, apatite and titanite, mineral phases that are more abundant in the pyroxene–hornblende gabbronorites. Early plagioclase fractionation results in an important increase of the bulk D_{Sr} . With continuing fractionation, the Unit I granite composition can readily be reproduced after ~70% fractionation (bulk $D_{Sr} = 2.4–2.6$, and bulk $D_{Nd} = 1.05–0.6$ respectively) from the estimated high-K calc-alkaline basaltic trachyandesitic parent magma composition.

We then tested whether FZ gabbronorites could correspond to the fractionated cumulate extracted during differentiation towards the FZ monzodiorites and Unit I granite. However, the exposed volumes of the Unit I granite (estimated to be ~18 km³ in the laccolith) and the associated feeder zone mafic cumulates (less than 1 km³ observed) are inconsistent with the modelled ratio ($F = 0.3$). This suggests that an important volume of the fractionated cumulates is not exposed today and probably remains in a deeper reservoir, as proposed by Michael (1991). In this model, the feeder zone mafic cumulates would represent the top of an ascending magma system, from which interstitial felsic magmas was extracted. The FZ layered gabbronorite leucocratic bands may then correspond to preserved interstitial liquid extraction channels.

Lower hornblende-gabbro—Unit III granite

We used AFC models to test whether the Unit III granite composition could have fractionated from the shoshonitic basaltic trachyandesitic starting magma composition. The hypothesis to be tested is whether felsic liquid can be extracted from the lower hornblende-gabbro sills to form the syn-magmatic Unit III granite. The Nd and Sr contents and isotopic compositions used in this model are given in Table 2.

There are no direct constraints for Unit III granites that would explain their radiogenic Sr isotopic signature. Based on the knowledge of the geology of the local Patagonian crust, assimilation of different country-rocks was considered. The Jurassic Patagonian batholith might be a suitable source rock to explain the contamination by a radiogenic Sr component. The Unit III granites are exposed close to the eastern margin of the batholith. The ¹⁴³Nd/¹⁴⁴Nd_t and ⁸⁷Sr/⁸⁶Sr_t of the Jurassic batholith (Hervé *et al.*, 2007) have been recalculated to 12.5 Ma, the crystallization age of the TPIC. Results are presented in Fig. 11. The Jurassic batholith model requires that the bulk D_{Nd} has to be close to ~1 (see Fig. 11a) to reproduce the Unit III granite composition. To also satisfy the ¹⁴³Nd/¹⁴⁴Nd vs ⁸⁷Sr/⁸⁶Sr trend of the TPIC granites (Fig. 11b), an assimilation/fractionation ratio of 0.25 is required (with bulk $D_{Nd} = 1$ and $D_{Sr} = 1$) to keep the

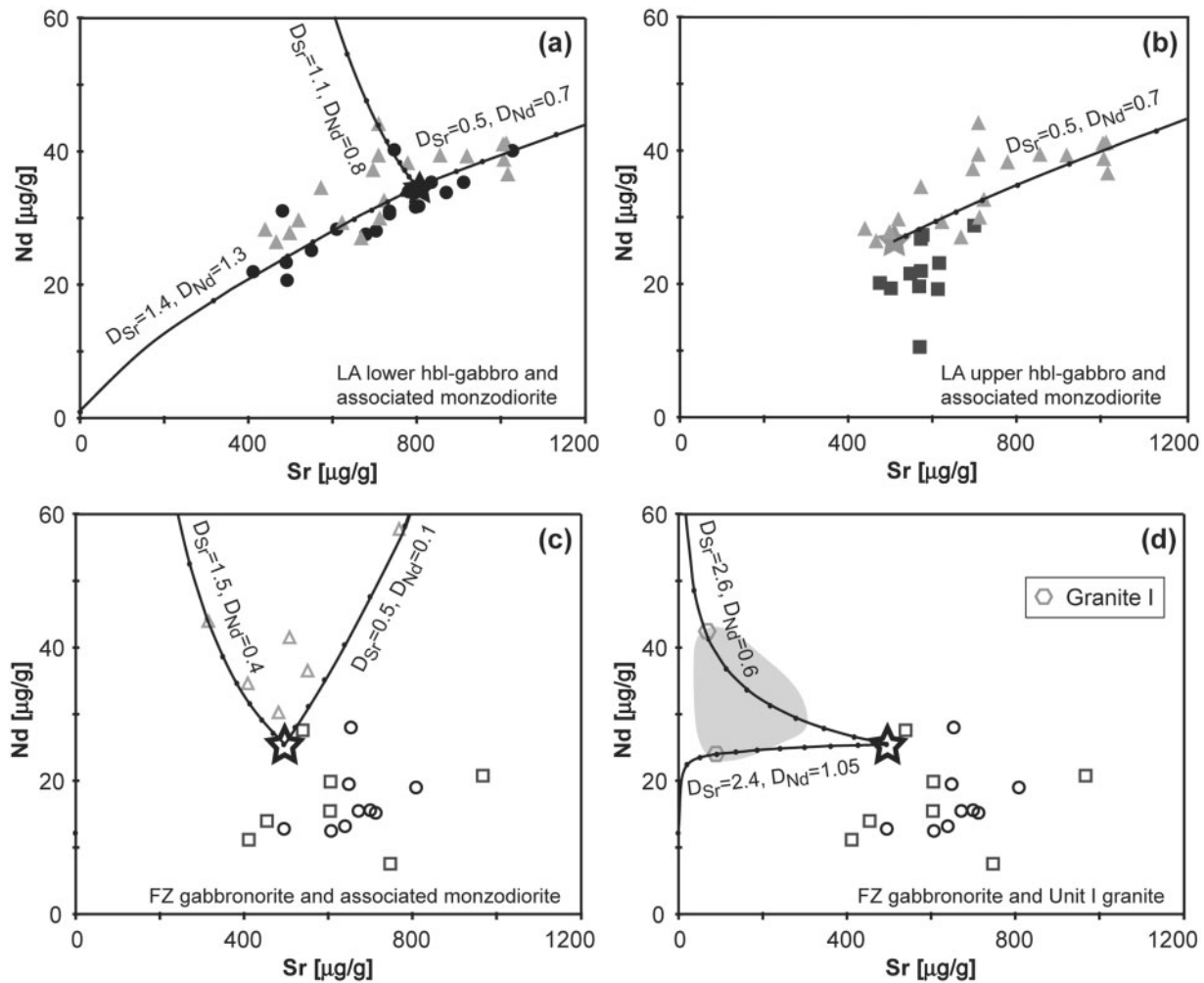


Fig. 10. Trace element variation diagrams showing fractional crystallization models using the IgPet software (Carr, 2012). (a) Modelled bulk Nd and Sr assuming a Nd- and Sr-rich parental liquid, as deduced from the dike compositions. It should be noted that the lower hornblende-gabbros and monzodiorites are similar in Nd and Sr and therefore a cumulate–residual liquid relationship is unlikely. (b) The Nd–Sr trend of the monzodiorites can reasonably be modelled by fractionating upper hornblende-gabbros. (c) Relationships between the high-K calc-alkaline basaltic trachyandesitic liquid, the feeder zone gabbronorite cumulates and the feeder zone monzodiorite; modelling indicates that the large variability in the monzodiorites can be explained by fractionating various modal proportions of mafic phases and plagioclase, determining the bulk D_{Sr} and D_{Nd} . (d) Simple fractionation models that test the relationship between Unit I granite and fractionating gabbronorite cumulates. The models require about 70% fractionation to fit the granite compositions. In both models Sr is highly compatible, indicating plagioclase fractionation. Tick marks represent 10% fractionation steps.

residual liquid fraction reasonably high (>0.2). To test this hypothesis, we modelled the $^{87}\text{Sr}/^{86}\text{Sr}$ vs Sr evolution from the LA alkali-rich primitive liquid to the TPIC granites (Fig. 11c). It appears that the necessary low D_{Sr} to maintain D_{Nd} reasonably low, cannot satisfy the TPIC evolution on the $^{87}\text{Sr}/^{86}\text{Sr}$ vs Sr diagram.

An r value of 0.25 corresponds to a reasonable maximum limit. An increase in bulk D_{Nd} and D_{Sr} is required if the r value is decreased. Nd is not compatible during fractional crystallization up to the saturation of light REE (LREE)-enriched accessory phases. It appears then to be difficult to model the Unit III granite by fractionation from the estimated shoshonitic basaltic trachyandesitic

parent liquid, concurrent with assimilation of the Jurassic Patagonian batholith.

Alternatively, assimilation of Patagonian S-type crust (Kilian & Behrmann, 2003) can be considered. Because of the strongly radiogenic Sr isotopic composition of Patagonian S-type crust at similar Sr contents, Sr needs to be incompatible to satisfy the Nd contents and Nd isotopic compositions ($D_{\text{Sr}}=0.6$ for $D_{\text{Nd}}=1.07$ and $r=0.25$) at the same time. This is clearly not the case (Fig. 7c).

Finally, we considered assimilation of Paleozoic metamorphic basement (Pankhurst *et al.*, 2003). However, the isotopic composition of the basement is not well constrained. We used two compositions: a Paleozoic schist,

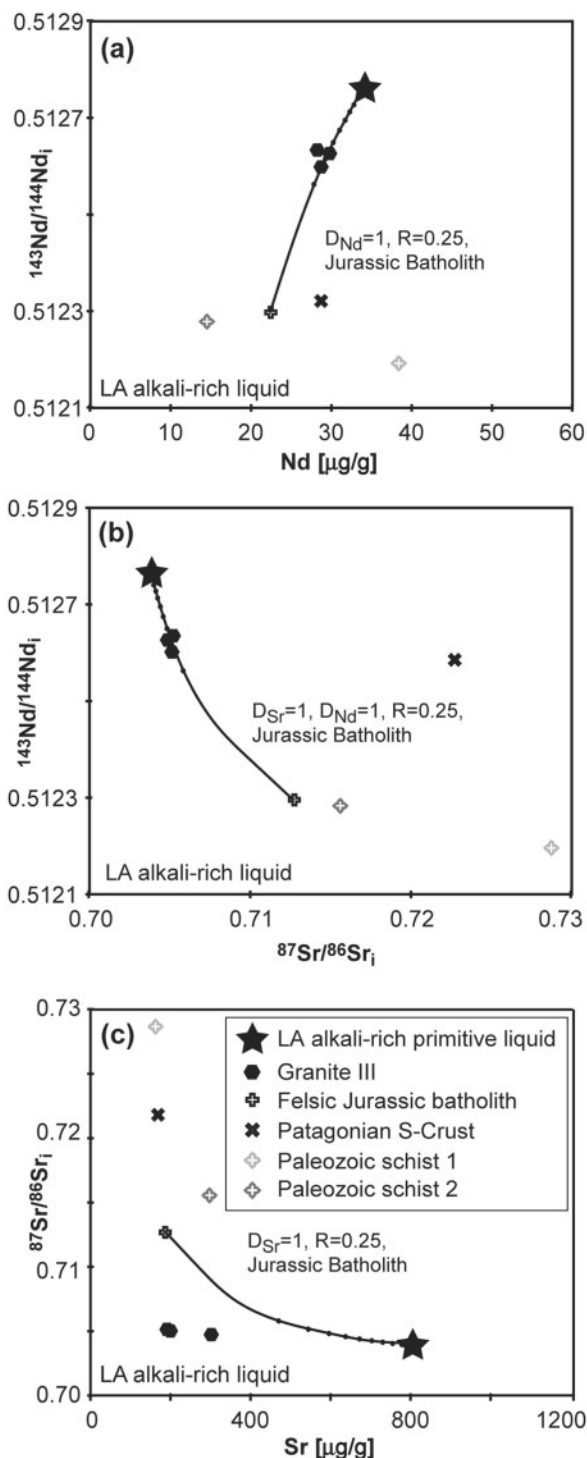


Fig. 11. AFC models calculated using IgPet software (Carr, 2012), using the Jurassic Patagonian Batholith (Hervé *et al.*, 2007) isotopic composition as assimilant and crystal fractionation from a shoshonitic basaltic trachyandesite liquid to produce the Unit III granite. Results show that in plots of Nd ($\mu\text{g g}^{-1}$) vs $^{143}\text{Nd}/^{144}\text{Nd}_i$ (a) and $^{87}\text{Sr}/^{86}\text{Sr}_i$ vs $^{143}\text{Nd}/^{144}\text{Nd}_i$ (b) the models reasonably reproduce the unit III granite, but they fail in $^{87}\text{Sr}/^{86}\text{Sr}_i$ vs Sr ($\mu\text{g g}^{-1}$). (c) Similar results are obtained for AFC models using Patagonian S-type crust or Paleozoic schists (not shown).

which is enriched in Sr and poor in Nd with less radiogenic Sr relative to Patagonian S-type crust, and a schist that is enriched in Nd and has a more radiogenic Sr isotopic composition (Pankhurst *et al.* 2003). AFC models using the first schist require bulk Nd to be incompatible ($D = 0.89$), with an r of 0.35, which is not realistic according to most thermal models (e.g. Matile *et al.* 2000). Assimilation of the second schist also fails to explain the observed isotopic compositions. On the one hand the model requires a low bulk D_{Sr} (~ 1) to satisfy the radiogenic isotope data ($D_{\text{Nd}} = 1.03$ and $r = 0.15$), and on the other hand a high bulk D_{Sr} (~ 2) is necessary to satisfy the $^{87}\text{Sr}/^{86}\text{Sr}$ vs Sr evolution. Thus, our AFC models indicate that a cogenetic link cannot be established between the shoshonitic lower hornblende-gabbro cumulates and the overlying Unit III granite.

CONCLUSIONS

Field, major and trace element, and Nd and Sr isotope data from the laccolith, the root zone and associated dikes indicate that the Torres del Paine mafic complex in Southern Patagonia formed from basaltic trachyandesitic parental magmas, with variable alkali and H_2O contents. Combined with U–Pb high-precision dating of zircons, the mafic rocks can in part be linked to the different granitic rocks of the laccolith. The compositional variability of the PMC gabbros is largely the result of olivine, clinopyroxene, orthopyroxene, \pm plagioclase \pm hornblende fractionation, with variable amounts of trapped interstitial melt. Simple trace element and AFC models allow us to distinguish three major fractionation series within the PMC, as follows.

(1) The FZ layered gabbronorite–FZ pyroxene–hornblende gabbronorite–FZ monzodiorite series displays Al_2O_3 enrichment and moderate positive Eu and Sr anomalies, which indicate that some of the residual liquid was extracted. Identical U–Pb zircon ages of granite unit I and the interstitial felsic melts of the gabbronorite allow for a link between these earliest magmas of the Torres del Paine igneous complex. We propose that segregation of granitic liquids was efficient during magma ascent through the feeder zone, at least for this early phase of magmatism, as evidenced by the dynamic and layered structure of the gabbronorites in this zone. The parent magma of the FZ gabbronorites was isotopically contaminated at an early stage, as evidenced by incomplete assimilation of deformed sedimentary xenoliths.

(2) The laccolith PMC is composed of two main fractionation series, each of them forming a layered sill complex with abundant evidence of incomplete segregation of interstitial felsic melts. The LA lower hornblende-gabbro is closely associated with alkali-rich monzodiorites. The latter occur as larger masses at the top and sometimes at the base of the hornblende-gabbro sills and form a

fine-grained groundmass. FC models fail to relate them as cumulate and residual liquid. Incomplete extraction of interstitial liquid explains the limited chemical variability between the hornblende-gabbros and monzodiorites. This makes FC models difficult to realize. We interpret the lower hornblende-gabbro chemistry and texture as a combination of fractionation prior to magma emplacement within the laccolith, with minor subsequent interstitial liquid extraction and continuing fractionation *in situ*. In contrast, the SiO₂-poor, alkali-rich, monzodiorite sills represent slowly cooled basaltic trachyandesitic liquids, compositionally similar to some of the dikes. Despite the age overlap with the overlying Unit III granite, no geochemical link could be established by crystal fractionation or AFC models, mainly because of the unknown composition of the potentially assimilated rocks,

(3) Finally, we have shown a geochemical link between the upper hornblende-gabbros and the alkali-poor monzodiorites in the laccolith. They formed during fractional crystallization from a high-K calc-alkaline basaltic trachyandesitic parent liquid. Crystal fractionation presumably started in a reservoir below the actual exposure level of the mafic rocks and continued after emplacement, within the laccolith.

We emphasize that detailed field observations coupled with high-precision U–Pb dating of zircons (Leuthold *et al.*, 2012) provides new perspectives on the interpretation of geochemical and radiogenic isotope data for shallow plutonic systems, in particular in areas where melt extraction is incomplete, such as the Torres del Paine mafic complex. Combining field observations, microtextural analyses, geochemical data and U–Pb zircon ages, we show that felsic liquid is expelled from mafic cumulates during magma ascent. It follows that crystal liquid separation is more efficient in subvertical, dynamic feeder systems whereas interstitial liquid remains largely trapped in subhorizontal sill complexes.

ACKNOWLEDGEMENTS

We thank J. Tuckermann for fruitful discussions and the possibility to use his samples. We thank M. Jutzeler and A. Vandelli for assistance during field work. Thanks go to J.-C. Lavanchy for help with XRF bulk-rock major element analyses and to A. Ulianov for help with the LA-ICP-MS. We are grateful to Tom Sisson for constructive discussions. We would like to acknowledge Chad Deering, Saskia Erdmann and Peter Michael for their constructive and detailed reviews. We thank the responsible authorities of CONAF (Corporación Nacional Forestal, Chile) for granting permission to collect in the Torres del Paine National Park and for their co-operation and hospitality.

FUNDING

Field work during the Paine Expeditions 2007 and 2008 was supported by grants from the Herbetta Foundation to O.M. We gratefully acknowledge the Swiss National Science Foundation (grant 20021-105421 and 20020-120120) to L.P.B. Finally, we acknowledge the Swiss Institute for Alpine Research for funding the 2007 expedition.

SUPPLEMENTARY DATA

Supplementary data for this paper are available at *Journal of Petrology* online.

REFERENCES

- Altenberger, U., Oberhaensli, R., Putlitz, B. & Wemmer, K. (2003). Tectonic controls of the Cenozoic magmatism at the Torres del Paine, southern Andes (Chile, 51°10'S). *Revista Geologica de Chile* **30**, 65–81.
- Baumgartner, L. P., Michel, J., Darbellay, B., Putlitz, B. & Robyr, M. (2006). The geology of the Torres del Paine laccolith, S Chile. *Backbone of the Americas—Patagonia to Alaska, Geological Society of America: Abstracts with Programs, Speciality Meeting, Mendoza, Argentina*, Paper no. 4-9.
- Baumgartner, L. P., Michel, J., Putlitz, B., Leuthold, J., Müntener, O., Robyr, M. & Darbellay, B. (2007). Field guide to the Torres del Paine Igneous Complex and its contact aureole. In: Demant, A., Hervé, F., Menichetti, M. & Tassone, A. (eds) *Field guide book GEOSUR 2007. Bolletino de Geofisica, GEOSUR 2007, International Congress on the Southern Hemisphere*. Santiago de Chile, 185 p.
- Boynton, W. V. (1984). Cosmochemistry of the rare earth elements: meteorite studies. In: Henderson, P. E. (ed.) *Rare Earth Element Geochemistry*. Amsterdam: Elsevier, pp. 63–114.
- Carr, M. (2012). *IGPET. Software Program*. Somerset, NJ: Terra Softa Inc.
- Chiaradia, M. (2009). Adakite-like magmas from fractional crystallization and melting–assimilation of mafic lower crust (Eocene Macuchi arc, Western Cordillera, Ecuador). *Chemical Geology* **265**, 468–487.
- Daly, R. A. (1925). The geology of Ascension Island. *Proceedings of the American Academy of Arts and Sciences* **60**(1), 3–80.
- Davidson, J., Turner, S., Handley, H., Macpherson, C. & Dosseto, A. (2007). Amphibole 'sponge' in arc crust? *Geology* **35**(9), 787–790.
- Davidson, J. P., De Silva, S. L., Holden, P. & Halliday, A. N. (1990). Small-scale disequilibrium in a magmatic inclusion and its more silicic host. *Journal of Geophysical Research* **93**(B11), 17661–17675.
- Debari, S., Kay, S. M. & Kay, R. W. (1987). Ultramafic xenoliths from Adagdak Volcano, Adak, Aleutian Islands, Alaska: deformed igneous cumulates from the Moho of an island arc. *Journal of Geology* **95**, 329–341.
- DePaolo, D. J. (1981). Trace element and isotopic effects of combined wallrock assimilation and fractional crystallization. *Earth and Planetary Science Letters* **53**, 189–202.
- de Saint-Blanquat, M., Horsman, E., Habert, G., Morgan, S., Vanderhaeghe, O., Law, R. & Tikoff, B. (2011). Multiscale magmatic cyclicality, duration of pluton construction, and the paradoxical relationship between tectonism and plutonism in continental arcs. *Tectonophysics* **500**, 20–33.
- Dessimo, M., Müntener, O. & Ulmer, P. (2012). A case for hornblende dominated fractionation of arc magmas: the Chelan Complex

- (Washington Cascades). *Contributions to Mineralogy and Petrology* **163**, 567–589.
- D’Orazio, M., Agostini, S., Mazzarini, F., Innocenti, F., Manetti, P., Haller, M. & Lahsen, A. (2000). The Pali Aike Volcanic Field, Patagonia: slab-window magmatism near the tip of South America. *Tectonophysics* **321**, 407–427.
- Dungan, M. A. & Davidson, J. (2004). Partial assimilative recycling of the mafic plutonic roots of arc volcanoes: An example from Chilean Andes. *Geology* **32**(9), 773–776.
- Fosdick, J. C., Romans, B. W., Fildani, A., Bernhardt, A., Calderón, M. N. & Graham, S. A. (2011). Kinematic evolution of the Patagonian retroarc fold-and-thrust belt and Magallanes foreland basin. *Geological Society of America Bulletin* **123**(9–10), 1679–1698.
- Glazner, A. F. (2007). Thermal limitations on the incorporation of wall rock into magma. *Geology* **35**(4), 319–322.
- Glazner, A. F. & Bartley, J. M. (2006). Is stopping a volumetrically significant pluton emplacement process? *Geological Society of America Bulletin* **118**(9/10), 1185–1195.
- Glazner, A. F., Bartley, J. M., Coleman, D. S., Gray, W. & Taylor, Z. (2004). Are plutons assembled over millions of years by amalgamation from small magma chambers? *Geological Society of America Today* **14**(4/5), 4–11.
- Gorring, M. L. & Kay, S. M. (2001). Mantle processes and sources of Neogene slab window magmas from southern Patagonia, Argentina. *Journal of Petrology* **42**(6), 1067–1094.
- Hervé, F., Pankhurst, R. J., Fanning, C., Calderon, M. & Yaxley, G. M. (2007). The South Patagonian Batholith; 150 my of granite magmatism on a plate margin. *Lithos* **97**, 373–394.
- Hildreth, W. & Moorbath, S. (1988). Crustal contributions to arc magmatism in the Andes of Central Chile. *Contributions to Mineralogy and Petrology* **98**(4), 455–489.
- Hofmann, A. W. (1997). Mantle geochemistry: the message from oceanic volcanism. *Nature* **385**, 219–229.
- Horsman, E., Morgan, S., de Saint-Blanquat, M., Habert, G., Nugent, A., Hunter, R. A. & Tikoff, B. (2010). Emplacement and assembly of shallow intrusions from multiple magma pulses, Henry Mountains, Utah. *Earth and Environmental Science Transactions of the Royal Society of Edinburgh* **100**, 117–132.
- Jackson, M. D. & Pollard, D. D. (1988). The laccolith–stock controversy: New results from the southern Henry Mountains, Utah. *Geological Society of America Bulletin* **100**(1), 117–139.
- Jackson, S. E., Longrich, H. P., Dunning, G. R. & Fryer, B. J. (1992). The application of laser-ablation microprobe–inductively coupled plasma–mass spectrometry (LAM–ICP–MS) to *in situ* trace-element determinations in minerals. *Canadian Mineralogist* **30**, 1049–1064.
- Jackson, S. E. (2008a). Calibration strategies for elemental analysis by LA–ICP–MS. In: Sylvester, P. (ed.) *Laser Ablation ICP–MS in the Earth Sciences: Current Practices and Outstanding Issues*. Mineralogical Association of Canada, Short Course Series **40**, 169–188.
- Jackson, S. E. (2008b). LAMTRACE data reduction software for LA–ICP–MS. In: Sylvester, P. (ed.) *Laser Ablation ICP–MS in the Earth Sciences: Current Practices and Outstanding Issues*. Mineralogical Association of Canada, Short Course Series **40**, 305–307.
- Jagoutz, O. E. (2010). Construction of the granitoid crust of an island arc. Part II: a quantitative petrogenetic model. *Contributions to Mineralogy and Petrology* **160**(3), 359–381.
- Karsten, J. L., Klein, E. M. & Sherman, S. B. (1996). Subduction zone geochemical characteristics in ocean ridge basalts from the southern Chile Ridge: Implications of modern ridge subduction systems for the Archean. *Lithos* **37**(2–3), 143–161.
- Kemp, A. I. S. (2004). Petrology of high-Mg, low-Ti igneous rocks of the Glenelg River Complex (SE Australia) and the nature of their interaction with crustal melts. *Lithos* **78**, 119–156.
- Kilian, R. & Behrmann, J. H. (2003). Geochemical constraints on the sources of Southern Chile Trench sediments and their recycling in arc magmas of the Southern Andes. *Journal of the Geological Society, London* **160**(1), 57–70.
- Kinzler, R. J., Grove, T. L. & Recca, S. I. (1990). An experimental study on the effect of temperature and melt composition on the partitioning of nickel between olivine and silicate melt. *Geochimica and Cosmochimica Acta* **54**, 1255–1265.
- Knesel, K. M., Davidson, J. P. & Duffield, W. A. (1999). Evolution of silicic magma through assimilation and subsequent recharge: Evidence from Sr isotopes and sanidine phenocrysts, Taylor Creek Rhyolite, NM. *Journal of Petrology* **40**(5), 773–786.
- Larocque, J. & Canil, D. (2010). The role of amphibole in the evolution of arc magmas and the crust: the case from the Jurassic Bonanza arc section, Vancouver Island, Canada. *Contributions to Mineralogy and Petrology* **159**, 475–492.
- Le Bas, M. J., Le Maitre, R. W., Streckeisen, A. & Zanettin, B. (1986). A chemical classification of volcanic rocks based on the total alkali–silica diagram. *Journal of Petrology* **27**, 745–750.
- Leuthold, J., Müntener, O., Baumgartner, L. P., Putlitz, B., Ovtcharova, M. & Schaltegger, U. (2012). Time resolved construction of a bimodal laccolith (Torres del Paine, Patagonia). *Earth and Planetary Science Letters* **325–326**, 85–92.
- Longrich, H. P., Günther, D. & Jackson, S. E. (1996). Elemental fractionation in laser ablation inductively coupled plasma–mass spectrometry. *Fresenius’ Journal of Analytical Chemistry* **355**, 538–542.
- Mason, P. R. D., Downes, H., Thirlwall, M. F., Seghedi, I., Szakacs, A., Lowry, D. & Mathey, D. (1996). Crustal assimilation as a major petrogenetic process in the East Carpathian Neogene and Quaternary continental margin arc, Romania. *Journal of Petrology* **37**(4), 927–959.
- Matile, L., Thomson, A. B. & Ulmer, P. (2000). A fractionation model for hydrous calc-alkaline plutons and the heat budget during fractional crystallization and assimilation. In: Bagdassarov, N., Laporte, D. & Thompson, A. B. (eds) *Lectures on the Physics and Chemistry of Partially Molten Rocks*. Dordrecht: Kluwer Academic, pp. 178–208.
- Michael, P. J. (1984). Chemical differentiation of the Cordillera Paine granite (southern Chile) by *in situ* fractional crystallization. *Contributions to Mineralogy and Petrology* **87**, 179–195.
- Michael, P. J. (1991). Intrusion of basaltic magma into a crystallizing granitic magma chamber: the Cordillera del Paine pluton in southern Chile. *Contributions to Mineralogy and Petrology* **108**(4), 396–418.
- Michel, J., Baumgartner, L. P., Bussy, F. & Putlitz, B. (2006). Initial data on the geochemistry of the Torres del Paine laccolith. *Backbone of the Americas—Patagonia to Alaska, Geological Society of America: Abstracts with Programs, Speciality Meeting, Mendoza, Argentina*, Paper no. 4–8.
- Michel, J., Baumgartner, L., de Saint-Blanquat, M., Putlitz, B., Sanchez, A., Darbellay, B. & Cavagna, M. (2007). Magnetic fabric of the Torres del Paine, Patagonia. *American Geophysical Union, Fall Meeting*, San Francisco, USA. Abstract #V33C-1524.
- Michel, J., Baumgartner, L., Putlitz, B., Schaltegger, U. & Ovtcharova, M. (2008). Incremental growth of the Patagonian Torres del Paine laccolith over 90 ky. *Geology* **36**(6), 459–465.
- Miller, C. F., Furbish, D. J., Walker, B. A., Claiborne, L. L., Koteas, G. C., Bleick, H. A. & Miller, J. S. (2011). Growth of plutons by incremental emplacement of sheets in crystal-rich host: Evidence from Miocene intrusions of the Colorado River region, Nevada, USA. *Tectonophysics* **500**(1–4), 65–77.

- Miller, J. S., Matzel, J. E. P., Miller, C. F., Burgess, S. D. & Miller, R. B. (2007). Zircon growth and recycling during the assembly of large, composite arc plutons. *Journal of Volcanology and Geothermal Research* **167**, 282–299.
- Müntener, O. & Ulmer, P. (2006). Experimentally derived high-pressure cumulates from hydrous arc magmas and consequences for the seismic velocity structure of lower arc crust. *Geophysical Research Letters* **33**, L21308.
- Müntener, O., Kelemen, P. B. & Grove, T. L. (2001). The role of H₂O during crystallization of primitive arc magmas under uppermost mantle conditions and genesis of igneous pyroxenites: an experimental study. *Contributions to Mineralogy and Petrology* **141**, 643–658.
- Pankhurst, R. J., Rapela, C. W., Loske, W. P., Márquez, M. & Fanning, C. M. (2003). Chronological study of the pre-Permian basement rocks of the southern Patagonia. *Journal of South American Earth Sciences* **16**, 27–44.
- Petford, N., Atherton, M. P. & Halliday, A. N. (1996). Rapid magma production rates, underplating and remelting in the Andes: isotopic evidence from northern-central Peru (9–11°S). *Journal of South American Earth Sciences* **9**(1–2), 69–78.
- Putlitz, B., Baumgartner, L. P., Oberhaensli, R., Diamond, L. & Altenberger, U. (2001). The Torres del Paine Laccolith (Chile); intrusion and metamorphism. In: *XI Annual V. M. Goldschmidt Proceedings*, Virginia, USA. Abstract 3534.
- Putlitz, B., Baumgartner, L. P. & Michel, J. (2006). Stable isotope systematic of the Torres del Paine Intrusive Complex (Patagonia, Chile). *Geological Society of America, Abstracts with Programs, Speciality Meeting* **2**, 104.
- Quensel, P. D. (1911). Geologisch-petrologische Studien in der patagonischen Cordillera. *Bulletin of the Geological Institute, University of Uppsala* **11**, 1–114.
- Sisson, T. W. & Grove, T. L. (1993). Experimental investigations of the role of H₂O in calc-alkaline differentiation and subduction zone magmatism. *Contributions to Mineralogy and Petrology* **113**, 143–166.
- Sisson, T. W., Grove, T. L. & Coleman, D. S. (1996). Hornblende gabbro sill complex at Onion Valley, California, and a mixing origin for the Sierra Nevada batholith. *Contributions to Mineralogy and Petrology* **126**, 81–108.
- Sisson, T. W., Ratajeski, K., Hankins, W. B. & Glazner, A. F. (2005). Voluminous granitic magmas from common basaltic sources. *Contributions to Mineralogy and Petrology* **148**, 635–661.
- Sun, S. S. & McDonough, W. F. (1989). Chemical and isotopic systematics of oceanic basalts: implications for mantle composition and processes. In: Saunders, A. D. & Norry, M. J. (eds) *Magmatism in the Ocean Basins. Geological Society London Special Publications* **42**, pp. 313–345.
- Tanaka, T., Togashi, S., Kamioka, H., Amakawa, H., Kagami, H., Hamamoto, T., Yuhara, M., Orihashi, Y., Yoneda, S., Shimizu, H., Kunimaru, T., Takahashi, K., Yanagi, Y., Nakano, T., Fujimaki, H., Shinjo, R., Asahara, Y., Tanimizu, M. & Dragusanu, C. (2000). JNdi-1: a neodymium isotopic reference in consistency with La Jolla neodymium. *Chemical Geology* **168**, 279–281.
- Todt, W., Cliff, R. A., Hanser, A. & Hofmann, A. W. (1996). Evaluation of a ²⁰²Pb–²⁰⁵Pb double spike for high-precision lead isotope analysis. In: Basu, A. & Hart, S. (eds) *Earth Processes: Reading the Isotopic Code. Geophysical Monograph, American Geophysical Union* **95**, 429–437.
- Ulmer, P. (1989). The dependence of the Fe²⁺–Mg cation-partitioning between olivine and basaltic liquid on pressure, temperature and composition: an experimental study to 30 kbars. *Contributions to Mineralogy and Petrology* **101**, 261–273.
- Ulmer, P., Callegari, E. & Sonderegger, U. C. (1983). Genesis of the mafic and ultramafic rocks and their genetical relations to the tonalitic–trondhjemitic granitoids of the southern part of the Adamello batholith, (Northern Italy). *Memorie della Società Geologica Italiana* **26**, 171–222.
- Upton, B. G. J., Skovgaard, A. C., McClurg, J., Kirstein, L., Cheadles, M., Emeleus, C. H., Wadsworth, W. J. & Fallick, A. E. (2002). Picritic magmas and the Rum ultramafic complex, Scotland. *Geological Magazine* **139**(4), 437–452.
- Vernon, R. H. (2004). *A Practical Guide to Rock Microstructure*. Cambridge: Cambridge University Press, 594 p.
- Wilson, T. J. (1983). Stratigraphic and structural evolution of the Ultima Esperanza foreland fold–thrust belt, Patagonian Andes, southern Chile. PhD thesis, Columbia University, New York, 360 p.